Electronic Supplementary Material (ESI) for Dalton Transactions.

SUPPLEMENTARY INFORMATION

Rhenium bipyridine catalysts with hydrogen bonding pendant amines for CO_2 reduction

Ashley N. Hellman, Ralf Haiges, Smaranda C. Marinescu*

Department of Chemistry, University of Southern California, Los Angeles, California 90089, United States
*Email: smarines@usc.edu

General Methods

All manipulations of air and moisture sensitive materials were conducted under a nitrogen atmosphere in a Vacuum Atmospheres drybox or on a dual manifold Schlenk line. The glassware was oven-dried prior to use. All solvents were degassed with nitrogen and passed through activated alumina columns and stored over 4Å Linde-type molecular sieves. Deuterated solvents were dried over 4Å Linde-type molecular sieves prior to use. Proton NMR spectra were acquired at room temperature using Varian (Mercury 400 2-Channel, VNMRS-500 2-Channel, VNMRS- 600 3-Channel, and 400-MR 2-Channel) spectrometers and referenced to the residual ^{1}H resonances of the deuterated solvent (^{1}H: $CDCl_3$) and are reported as parts per million relative to tetramethylsilane. Elemental analyses were performed using Thermo Scientific™ FLASH 2000 CHNS/O Analyzers. All the chemical reagents were purchased from commercial vendors and used without further purification.

Electrochemistry experiments were carried out using a Pine potentiostat. The experiments were performed in a single compartment electrochemical cell under nitrogen or CO_2 atmosphere using a 3 mm diameter glassy carbon electrode as the working electrode, a platinum wire as auxiliary electrode and a silver wire as the reference electrode. Ohmic drop was compensated using the postive feedback compensation implemented in the instrument. All electrochemical experiments were performed with iR compensation using the current interrupt (RUCI) method in AfterMath. Typical values for the cell resistance were around 0.16-0.17 ohms. All experiments in this paper were referenced relative to ferrocene (Fc) with the $Fe^{3+/2+}$ couple at 0.0 V. Alternatively, in cases when the redox couple of ferrocene overlapped with other features of interest, decamethylferrocene (Fc*) was used as an internal standard with the $Fe^{*3+/2+}$ couple at –0.48 V. All electrochemical experiments were performed with 0.1 M tetrabutylammonium hexafluorophosphate as supporting electrolyte. The concentrations of the rhenium catalysts were generally at 1 mM and experiments with CO_2 were performed at gas saturation in acetonitrile (MeCN) or dimethylformamide (DMF).

Controlled-potential electrolysis measurements were conducted in a two-chamber H cell. The first chamber held the working and reference electrodes in 40 mL of 0.1 M tetrabutylammonium hexafluorophosphate and TFE in MeCN or DMF. The second chamber held the auxiliary electrode in 25 mL of 0.1 M tetrabutylammonium hexafluorophosphate in MeCN or DMF. The two chambers were separated by a fine porosity glass frit. The reference electrode was placed in a separate compartment and connected by a Vycor tip. Glassy carbon plate electrodes (6 cm × 1 cm × 0.3 cm; Tokai Carbon USA) were used as the working and auxiliary electrodes. Using a gas-tight syringe, 2 mL of gas were withdrawn from the headspace of the H cell and injected into a gas chromatography instrument (Shimadzu GC-2010-Plus) equipped with a BID detector and a Restek ShinCarbon ST Micropacked column. Faradaic efficiencies were determined by diving the measured CO produced by the amount of CO expected based on the charge passed during the bulk electrolysis experiment. For each species the controlled-potential electrolysis measurements were performed at least twice, leading to similar behavior. The reported Faradaic efficiencies and mmol of CO produced are average values.

Experimental

Synthesis of *N*^{6},*N*$^{6'}$-dimethyl-[2,2'-bipyridine]-6,6'-diamine (L^1).

A high pressure flask was charged with 6,6'-dibromo-2,2'-bipyridine (105 mg, 0.33 mmol), CuI (6.3 mg, 0.033 mmol), L-proline (7.8 mg. 0.067 mmol), and Na_2CO_3 (110 mg, 1 mmol). Subsequently, 1 mL DMSO and 0.1 mL water were added, and the solution was purged under N_2 for five minutes while stirring. Methylamine (2 mL, 50 mM) was added via syringe, and the flask was sealed. The reaction mixture was heated to 130 °C and allowed to stir for 24 hours. After cooling, the organic phase was extracted with ethyl acetate and washed with copious amounts of water. The organic phase was dried over Na_2SO_4, and the solvent was removed by rotary evaporation. The product was obtained as a yellow-brown solid in approximately 70% yield. ^1H NMR ($CDCl_3$): δ 7.63 (d, 1H, NC_5H_3), 7.54 (t, 1H, *p*-NC_5H_3), 6.40 (d, 1H, NC_5H_3), 4.55 (s, 1H, N*H*), 2.98 (d, 3H, NCH_3) ppm.

Synthesis of *N*-methyl-[2,2'-bipyridin]-6-amine (L^2).

A high pressure flask was charged with 6-bromo-2,2'-bipyridine (160 mg, 0.67 mmol), CuI (6.3 mg, 0.033 mmol), L-proline (7.8 mg, 0.067 mmol), and Na_2CO_3 (110 mg, 1 mmol). Subsequently, 1 mL DMSO and 0.1 mL water were added, and the solution was purged under N_2 for five minutes while stirring. Methylamine (2 mL, 50 mM) was added via syringe, and the flask was sealed. The reaction mixture was heated to 130 °C and allowed to stir for 48 hours. After cooling, the organic phase was extracted with ethyl acetate and washed with copious amounts of water. The organic phase was dried over Na_2SO_4, and the solvent was removed by rotary evaporation. The product was obtained as a yellow-brown solid in approximately 72% yield. ^1H NMR ($CDCl_3$): δ 8.65 (d, 1H,

NC_5H_3), 8.33 (d, 1H, NC_5H_3), 7.78 (t, 1H, *p*-NC_5H_3), 7.68 (d, 1H, NC_5H_3), 7.58 (t, 1H, *p*-NC_5H_3), 6.45 (d, 1H, NC_5H_3), 4.58 (s, 1H, N*H*), 3.01 (d, 3H, NCH_3) ppm.

Synthesis of N^6,N^6,$N^{6'}$,$N^{6'}$-tetramethyl-[2,2'-bipyridine]-6,6'-diamine (L^3).
A high pressure flask was charged with 6,6'-dibromo-2,2'-bipyridine (105 mg, 0.33 mmol), CuI (6.3 mg, 0.033 mmol), L-proline (7.8 mg, 0.067 mmol), and Na_2CO_3 (110 mg, 1 mmol). Subsequently, 1 mL DMSO and 0.1 mL water were added, and the solution was purged under N_2 for five minutes while stirring. Dimethylamine (2 mL, 30 mM) was added via syringe, and the flask was sealed. The reaction mixture was heated to 130 °C and allowed to stir for 48 hours. After cooling, the organic phase was extracted with ethyl acetate and washed with copious amounts of water. The organic phase was dried over Na_2SO_4, and the solvent was removed by rotary evaporation. The product was obtained as an orange-brown solid in approximately 56% yield. ^{1}H NMR ($CDCl_3$): δ 7.71 (d, 1H, NC_5H_3), 7.56 (t, 1H, *p*-NC_5H_3), 6.53 (d, 1H, NC_5H_3), 3.16 (s, 6H, $N(CH_3)_2$) ppm.

Synthesis of *N*,*N*-dimethyl-[2,2'-bipyridin]-6-amine (L^4).
A high pressure flask was charged with 6-bromo-2,2'-bipyridine (160 mg, 0.67 mmol), CuI (6.3 mg, 0.033 mmol), L-proline (7.8 mg, 0.067 mmol), and Na_2CO_3 (110 mg, 1 mmol). Subsequently, 1 mL DMSO and 0.1 mL water were added, and the solution was purged under N_2 for five minutes while stirring. Dimethylamine (2 mL, 30 mM) was added via syringe, and the flask was sealed. The reaction mixture was heated to 130 °C and allowed to stir for 48 hours. After cooling, the organic phase was extracted with ethyl acetate and washed with copious amounts of water. The organic phase was dried over Na_2SO_4, and the solvent was removed by rotary evaporation. The product was obtained as an orange-brown solid in approximately 78% yield. ^{1}H NMR ($CDCl_3$): δ 8.64 (d, 1H, NC_5H_3), 8.41 (d, 1H, NC_5H_3), 7.77 (t, 1H, *p*-NC_5H_3), 7.69 (d, 1H, NC_5H_3), 7.59 (t, 1H, *p*-NC_5H_3), 7.25 (d, 1H, NC_5H_3), 6.57 (d, 1H, NC_5H_3), 3.16 (s, 6H, $N(CH_3)_2$) ppm.

Synthesis of $Re(L^1)(CO)_3Cl$ (1).
A three neck flask was charged under N_2 with ligand $\mathbf{L^1}$ (102 mg) and rhenium pentacarbonyl chloride (165 mg, 1 eq.). While stirring, dry toluene (20 mL) was added via syringe. The reaction mixture was heated to reflux and allowed to stir overnight. After cooling, yellow solid precipitated, which was collected by vacuum filtration and washed with diethyl ether. The filtrate was transferred to a jar that was capped and placed in the freezer to allow more solid to precipitate from solution. The total yield of bright yellow powder (complex **1**) was approximately 95%. Yellow crystals suitable for X-ray diffraction were grown from diffusion of diethyl ether into a dimethylformamide (DMF) solution of **1**. ^{1}H NMR ($CDCl_3$): δ 7.70 (t, 1H, *p*-NC_5H_3), 7.32 (d, 1H, NC_5H_3), 6.66 (d, 1H, NC_5H_3), 6.23 (s, 1H, N*H*), 3.07 (s, 3H, NCH_3) ppm. Anal. Calcd. for **1**: C, 34.65; H, 2.71; N, 10.78. Found: C, 34.68; H, 2.63; N, 10.63.

Synthesis of $Re(L^2)(CO)_3Cl$ (2).
A three neck flask was charged under N_2 with ligand $\mathbf{L^2}$ (168 mg) and rhenium pentacarbonyl chloride (235 mg, 1 eq.). While stirring, dry toluene (35 mL) was added via syringe. The reaction mixture was heated to reflux and allowed to stir overnight.

After cooling, yellow solid precipitated, which was collected by vacuum filtration and washed with diethyl ether. The filtrate was transferred to a jar that was capped and placed in the freezer to allow more solid to precipitate from solution. The total yield of bright yellow powder (complex **2**) was approximately 97%. Yellow crystals suitable for X-ray diffraction were grown from diffusion of diethyl ether into a dimethylformamide (DMF) solution of **2**. ^{1}H NMR ($CDCl_3$): δ 9.04 (d, 1H, NC_5H_3), 8.06 (d, 1H, NC_5H_3), 7.99 (t, 1H, p-NC_5H_3), 7.75 (t, 1H, p-NC_5H_3), 7.45 (m, 2H, NC_5H_3), 6.74 (d, 1H, NC_5H_3), 6.09 (s, 1H, N*H*), 3.10 (d, 3H, NCH_3). Anal. Calcd. for **2**: C, 34.25; H, 2.26; N, 8.56. Found: C, 34.11; H, 2.28; N, 8.38.

Synthesis of Re(L^3)$(CO)_3$Cl (3).

A three neck flask was charged under N_2 with ligand **L^3** (149 mg) and rhenium pentacarbonyl chloride (271 mg, 1 eq.). While stirring, dry toluene (40 mL) was added via syringe. The reaction mixture was heated to reflux and allowed to stir overnight. After cooling, orange solid precipitated, which was collected by vacuum filtration and washed with diethyl ether. The filtrate was transferred to a jar that was capped and placed in the freezer to allow more solid to precipitate from solution. The total yield of bright orange powder (complex **3**) was approximately 94%. Orange crystals suitable for X-ray diffraction were grown from diffusion of diethyl ether into a dimethylformamide (DMF) and chloroform solution of **3**. ^{1}H NMR ($CDCl_3$): δ 7.89 (t, 1H, p-NC_5H_3), 7.65 (d, 1H, NC_5H_3), 7.18 (d, 1H, NC_5H_3), 3.07 (s, 6H, $N(CH_3)_2$). Anal. Calcd. for **3**: C, 37.26; H, 3.31; N, 10.22. Found: C, 37.07; H, 3.22; N, 9.87.

Synthesis of Re(L^4)$(CO)_3$Cl (4).

A three neck flask was charged under N_2 with ligand **L^4** (105 mg) and rhenium pentacarbonyl chloride (158 mg, 1 eq.). While stirring, dry toluene (20 mL) was added via syringe. The reaction mixture was heated to reflux and allowed to stir overnight. After cooling, orange solid precipitated and was collected by vacuum filtration and washed with diethyl ether. The filtrate was transferred to a jar that was capped and placed in the freezer to allow more solid to precipitate from solution. The total yield of bright orange powder (complex **4**) was approximately 99%. Orange crystals suitable for X-ray diffraction were grown from diffusion of diethyl ether into a dimethylformamide (DMF) solution of **4**. ^{1}H NMR ($CDCl_3$): δ 9.08 (d, 1H, NC_5H_3), 8.03 (m, 2H, NC_5H_3), 7.89 (t, 1H, p-NC_5H_3), 7.67 (d, 1H, NC_5H_3), 7.48 (t, 1H, p-NC_5H_3), 7.18 (d, 1H, NC_5H_3), 6.57 (d, 1H, NC_5H_3), 3.12 (s, 6H, $N(CH_3)_2$). Anal. Calcd. for **4**: C, 35.68; H, 2.60; N, 8.32. Found: C, 35.79; H, 2.67; N, 8.30.

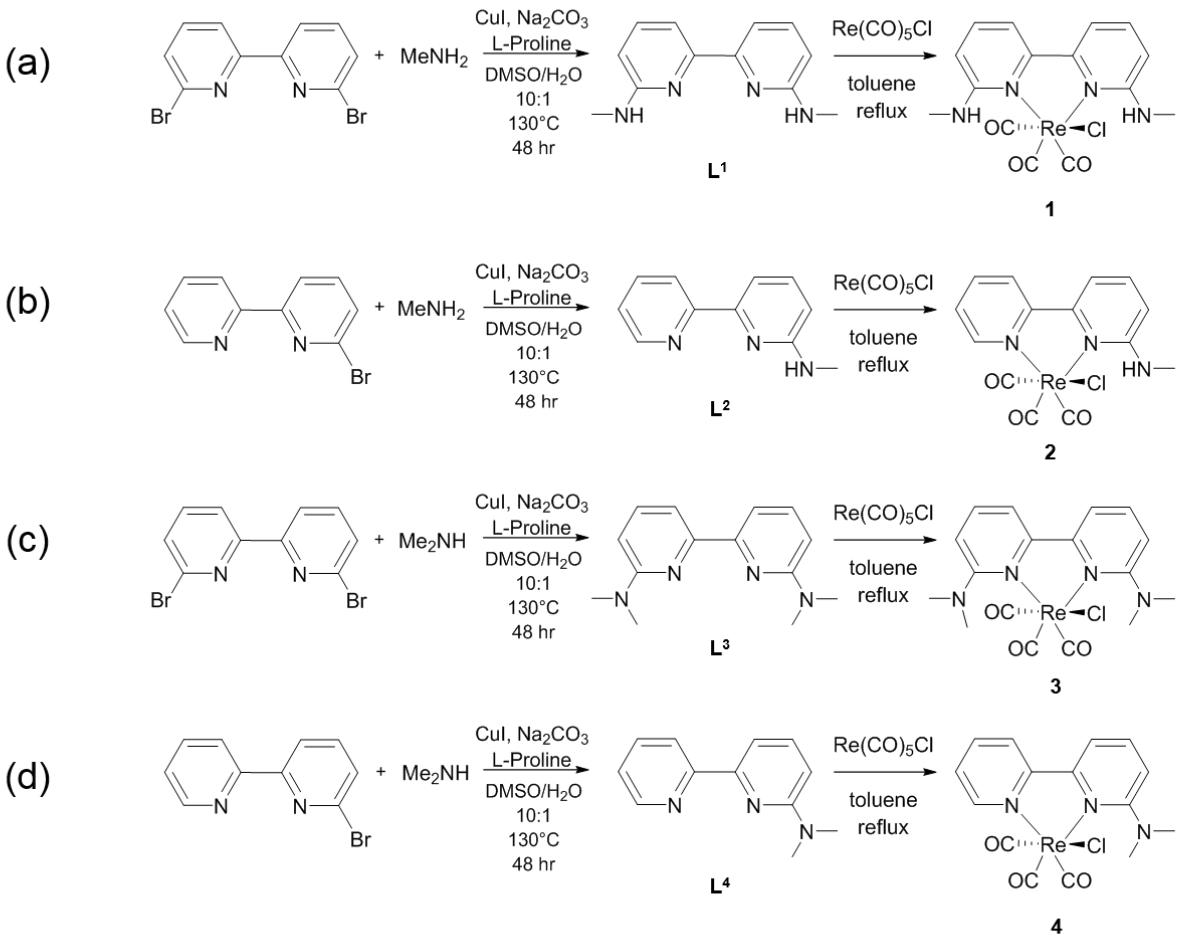

Scheme S1. Synthetic schemes for (a) **1**, (b) **2**, (c) **3**, and (d) **4**.

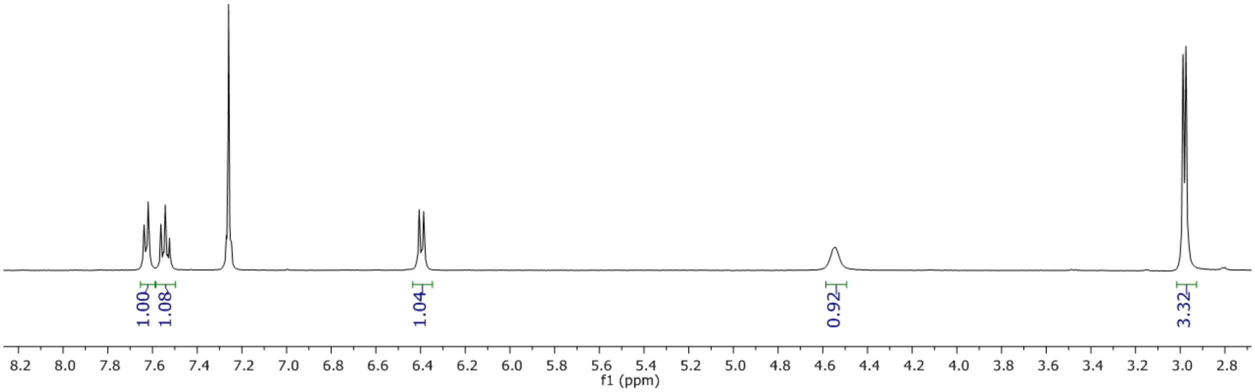

Figure S1: 400 MHz ^{1}H NMR spectrum of ligand $\mathbf{L^1}$ in $CDCl_3$.

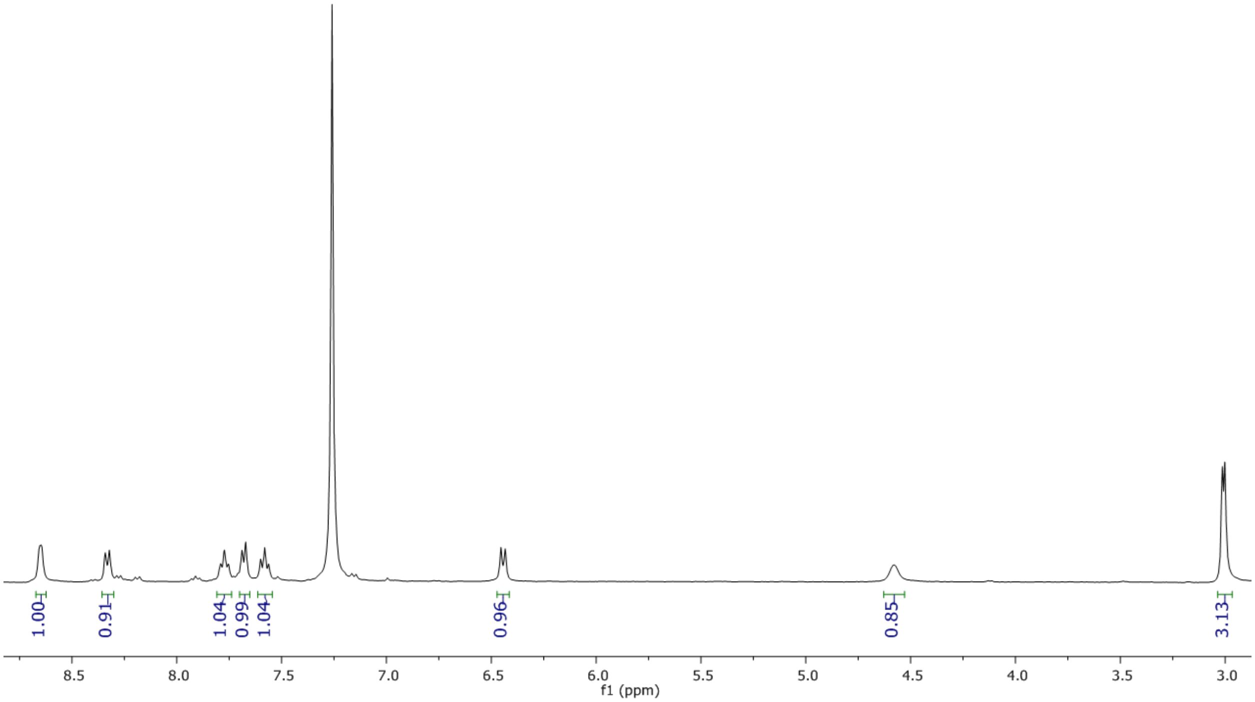

Figure S2: 400 MHz ^{1}H NMR spectrum of ligand $\mathbf{L^2}$ in $CDCl_3$.

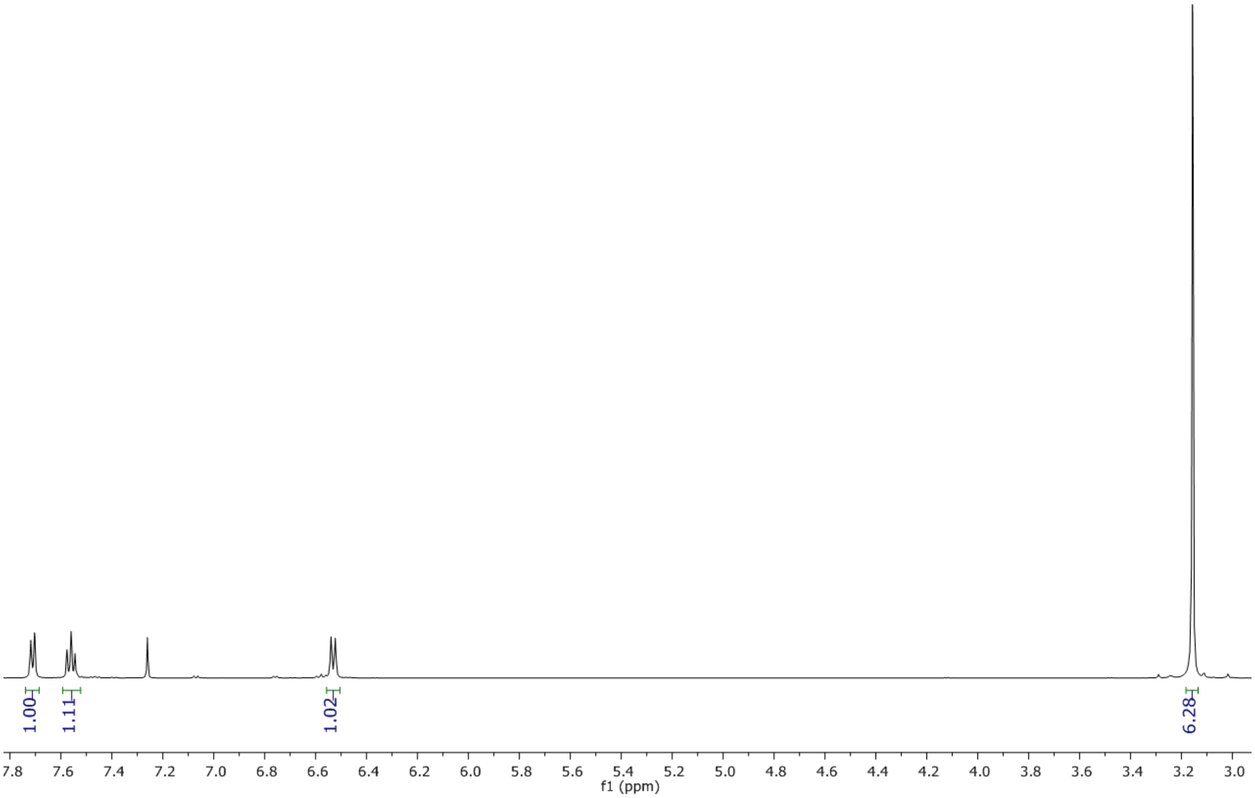

Figure S3: 500 MHz ^{1}H NMR spectrum of ligand $\mathbf{L^3}$ in $CDCl_3$.

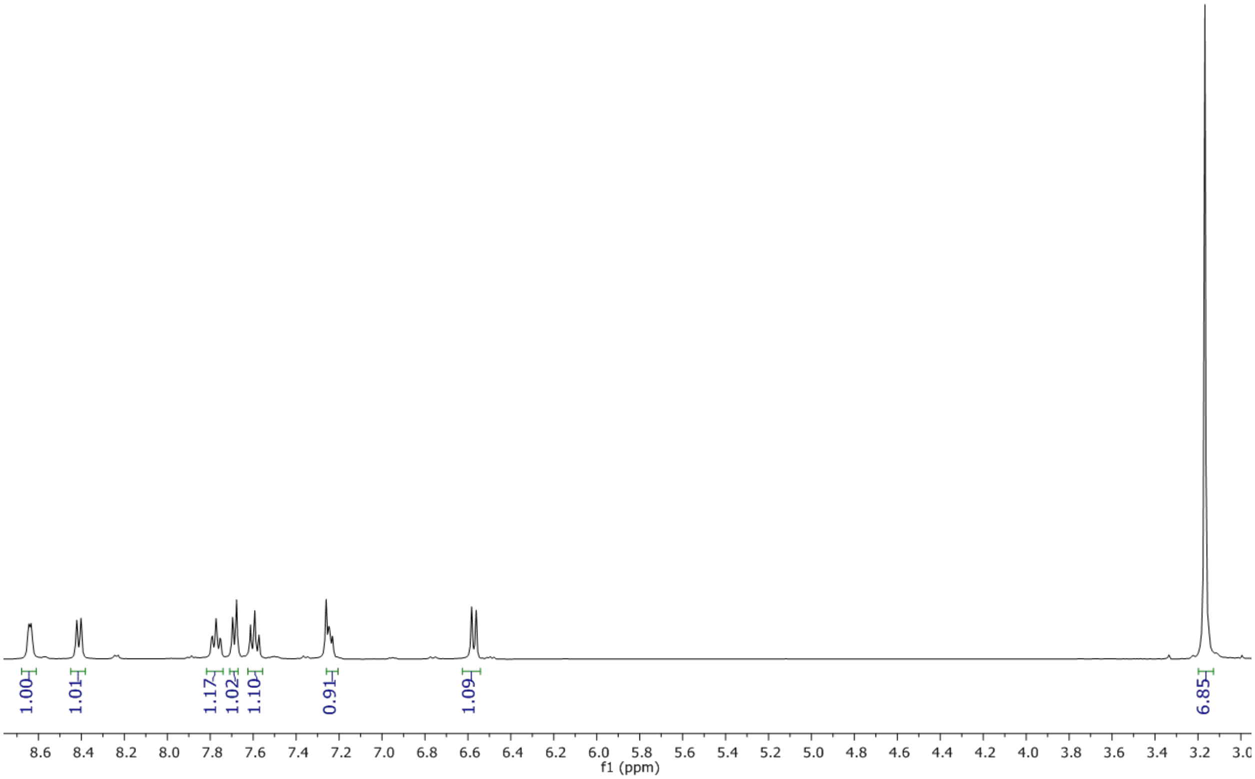

Figure S4: 400 MHz ^{1}H NMR spectrum of ligand $\mathbf{L^4}$ in $CDCl_3$.

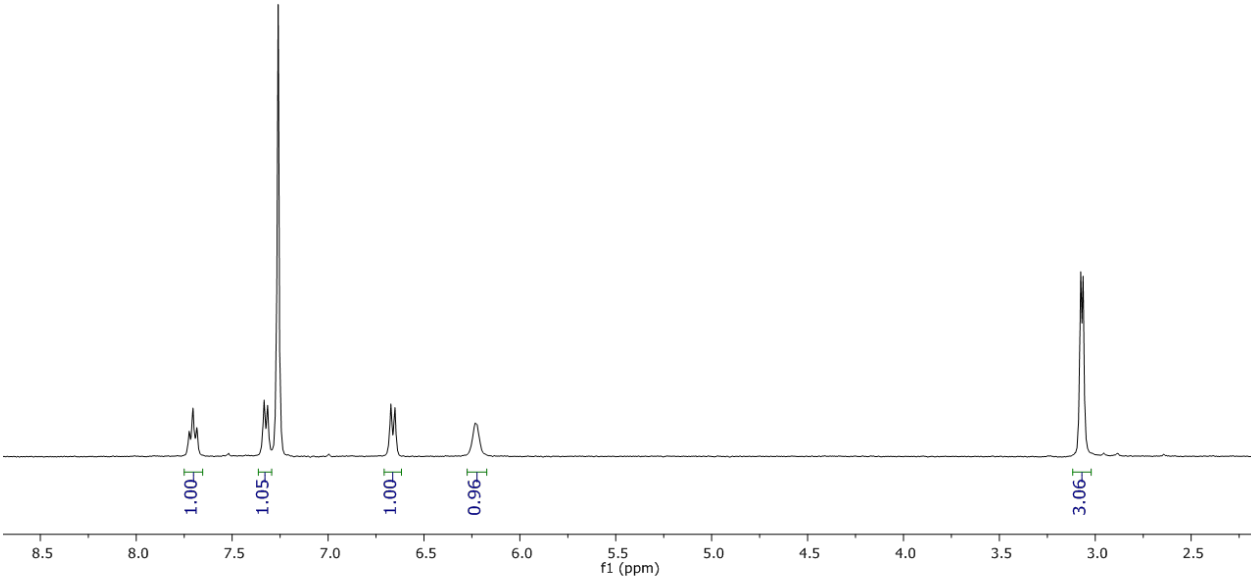

Figure S5: 400 MHz ^{1}H NMR spectrum of complex **1** in $CDCl_3$.

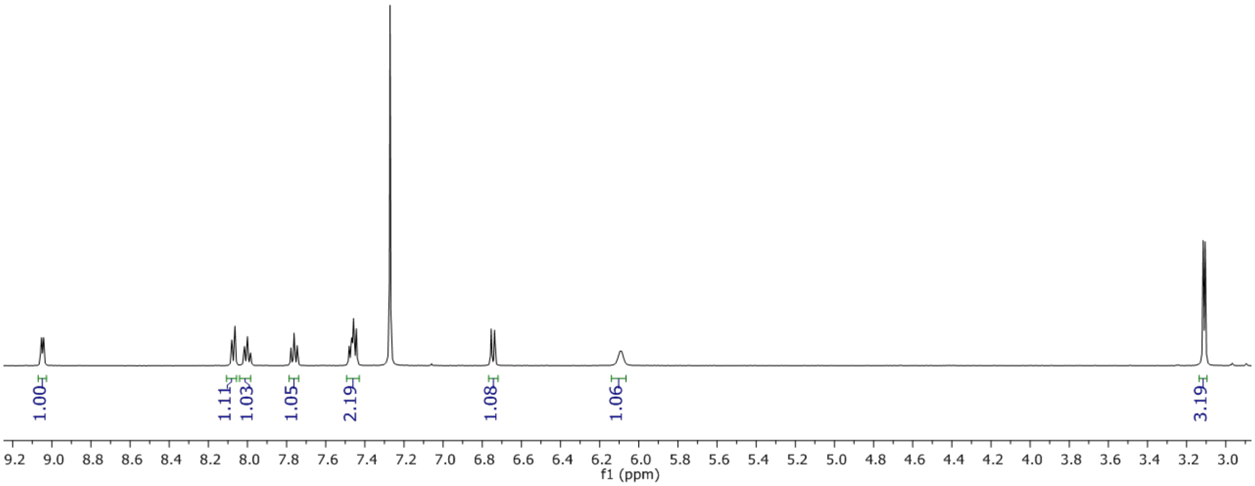

Figure S6: 500 MHz ^{1}H NMR spectrum of complex **2** in $CDCl_3$.

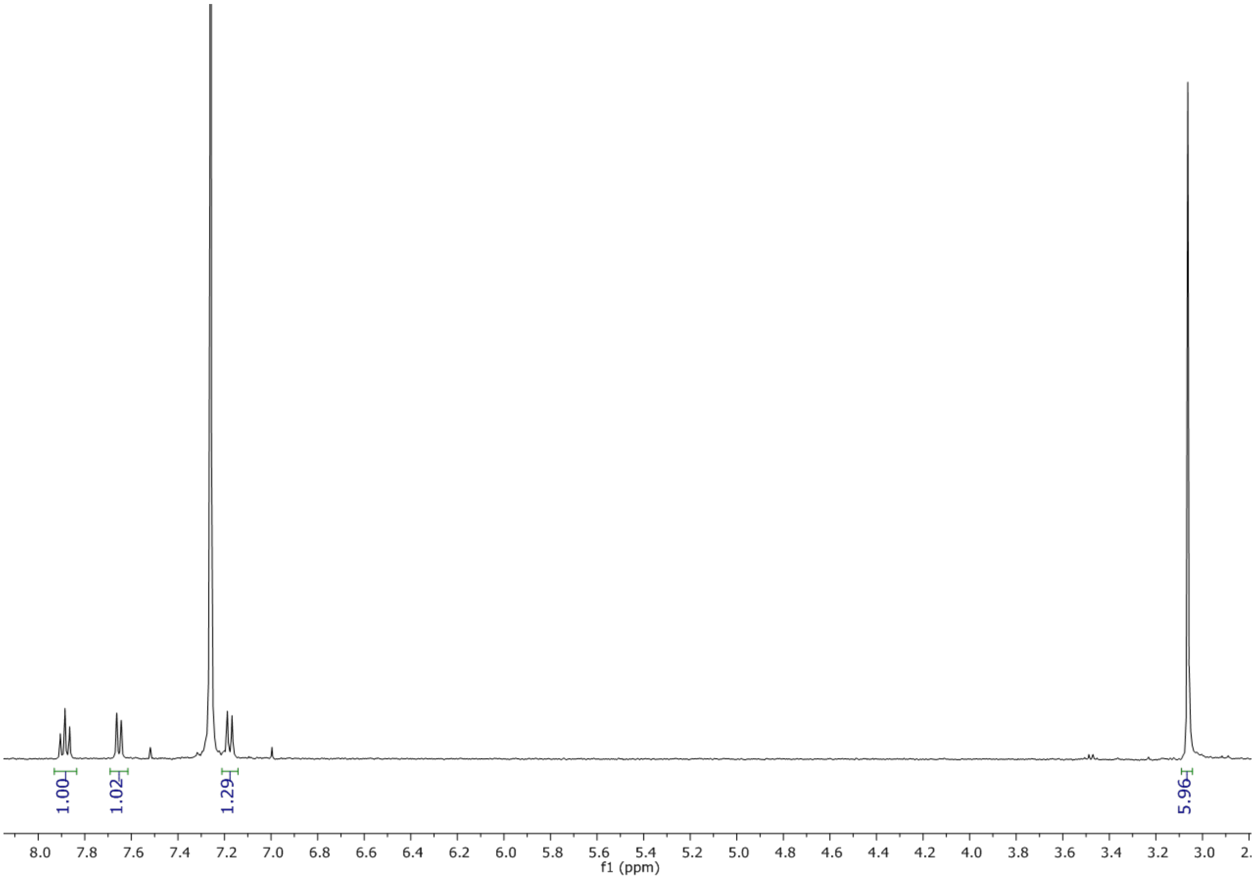

Figure S7: 400 MHz ^{1}H NMR spectrum of complex **3** in $CDCl_3$.

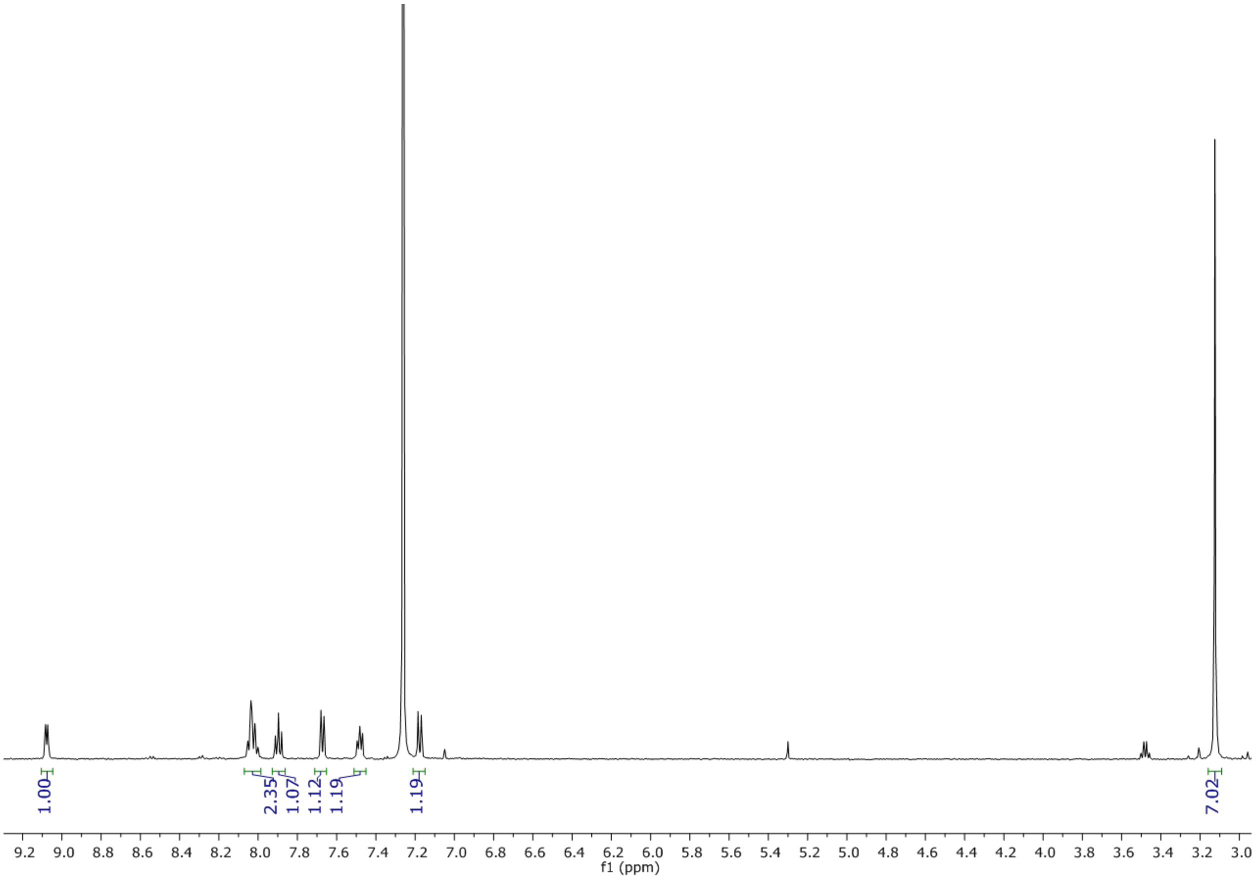

Figure S8: 500 MHz ^{1}H NMR spectrum of complex **4** in $CDCl_3$.

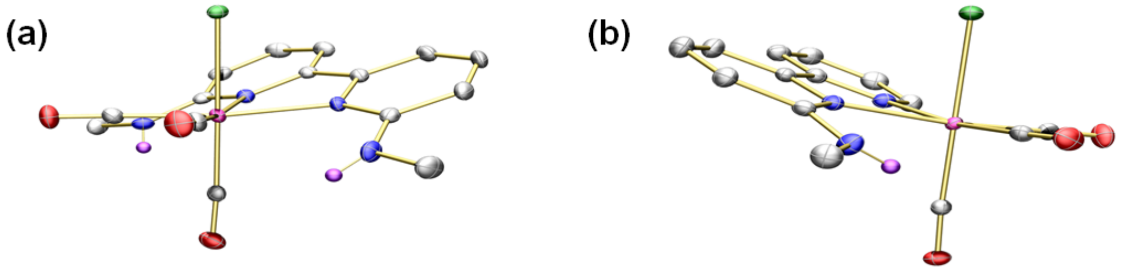

Figure S9. Solid state structures of (a) **1** and (b) **2** with N-H bonds included. Color legend of the atoms: gray – C; blue – N; red – O; green – Cl; pink – Re; purple – H. Solvent molecules and additional hydrogen atoms are excluded for clarity.

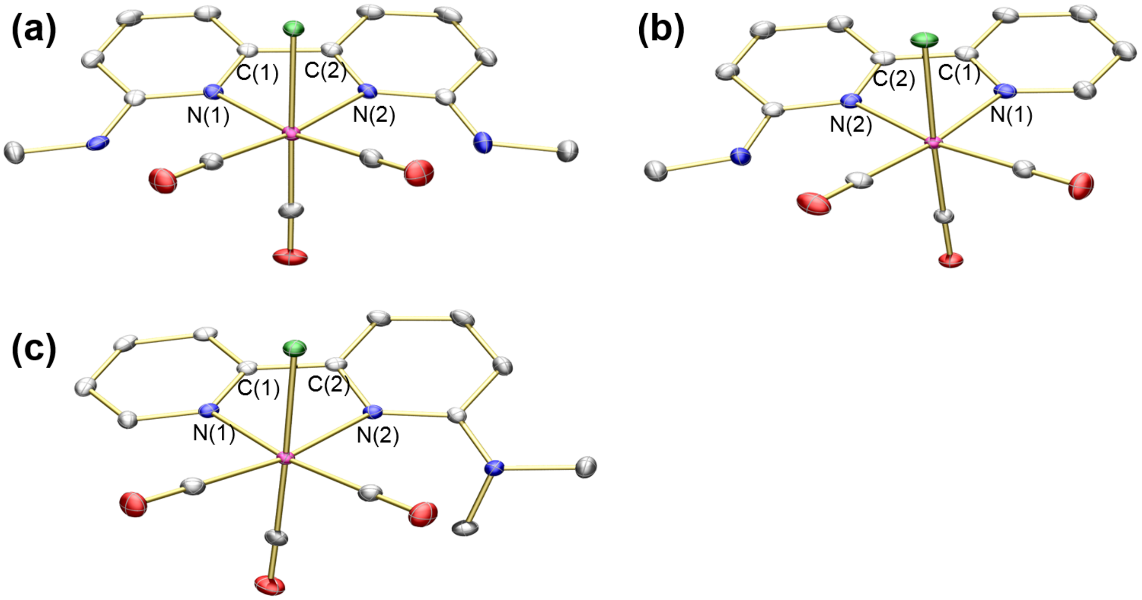

Figure S10. Solid state structures of (a) **1**, (b) **2**, and (c) **4** showing labels for the nitrogen and carbon atoms involved in the N—C—C—N torsion angles. Color legend of the atoms: gray – C; blue – N; red – O; green – Cl; pink – Re. Solvent molecules and additional hydrogen atoms are excluded for clarity.

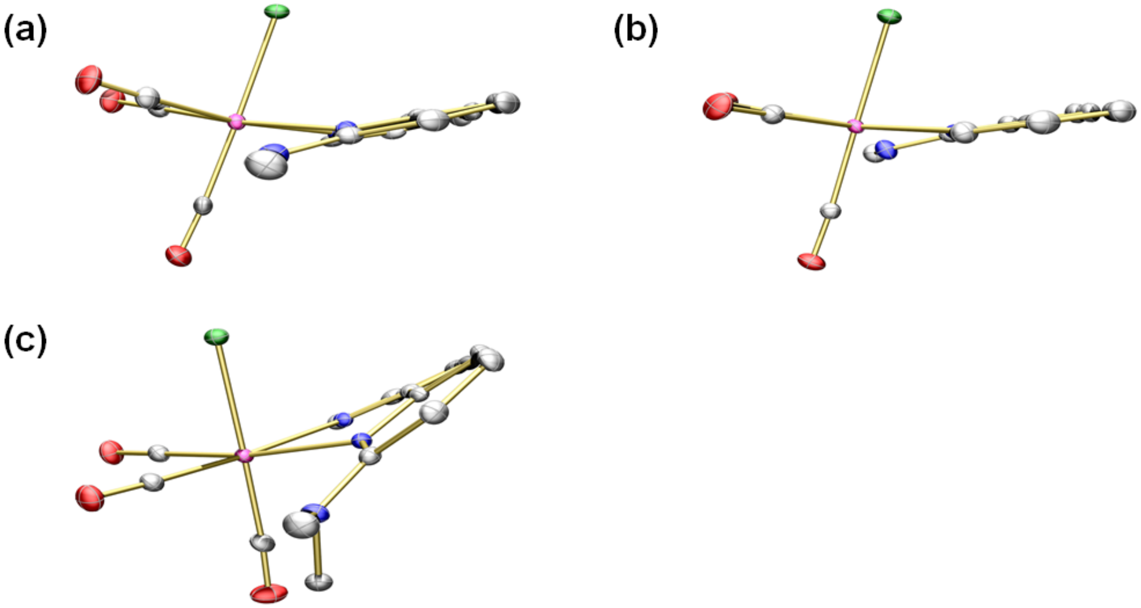

Figure S11. Solid state structures of (a) **1**, (b) **2**, and (c) **4** showing torsion angles of the N—C—C—N bonds. Color legend of the atoms: gray – C; blue – N; red – O; green – Cl; pink – Re. Solvent molecules and hydrogen atoms are excluded for clarity.

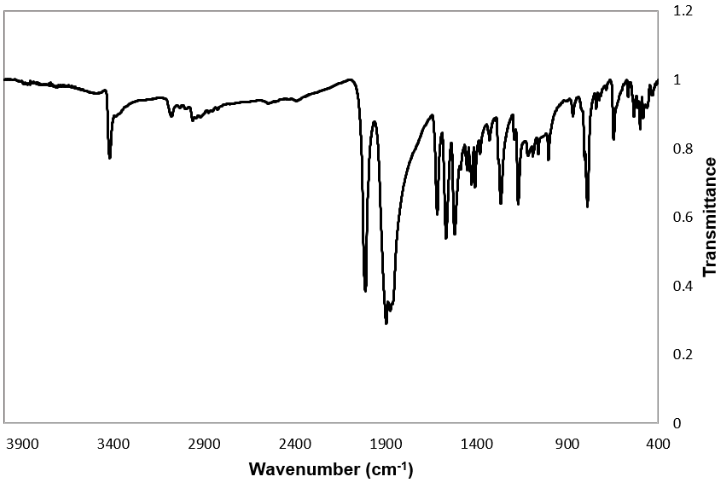

Figure S12: FT-IR spectrum of complex **1**.

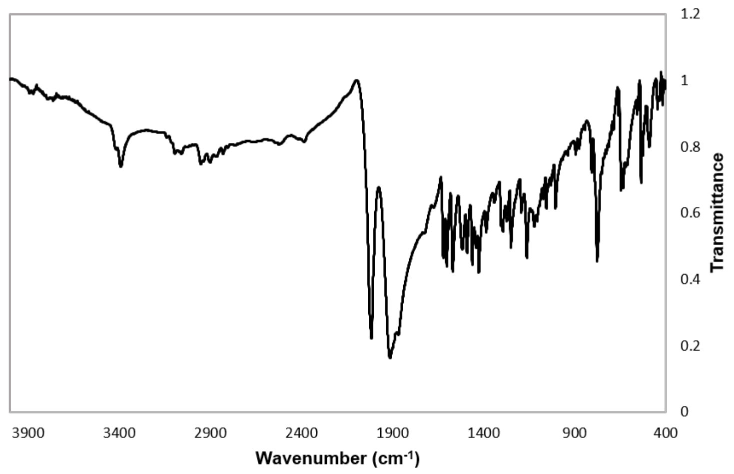

Figure S13: FT-IR spectrum of complex **2**.

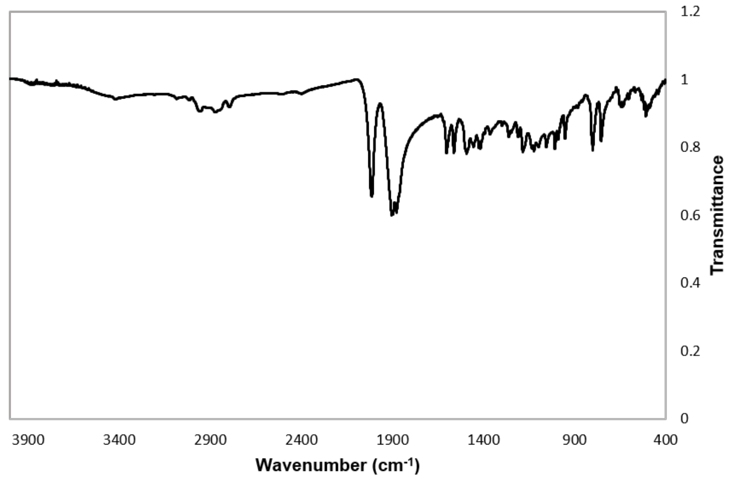

Figure S14: FT-IR spectrum of complex **3**.

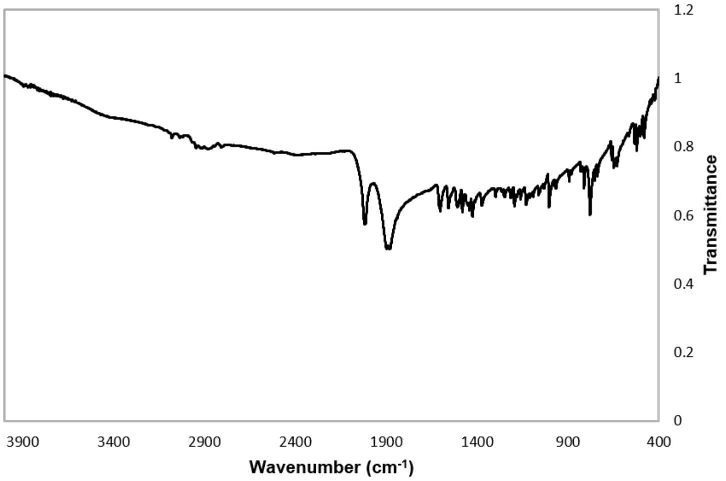

Figure S15: FT-IR spectrum of complex **4**.

Complex	N-H	C=O (a_1')	C=O (a")	C=O (a_2')
1	3416	2011	1897	1857
2	3391	2014	1915	1869
3	–	2013	1903	1876
4	–	2016	1899	1880

Table S1. Pertinent IR spectroscopy wavenumbers for complexes **1**–**4**.

Catalyst	1st reduction	Add’l reduction	2nd reduction
1	-1.96	-2.05	-2.25
2	-1.87	-2.01	-2.16
3	-1.92	–	-2.26
4	-1.84	–	-2.19

Table S2. Reduction potentials (V vs. $Fc^{+/0}$) for catalysts **1** through **4** under N_2. Scan rate: 100 mV/s.

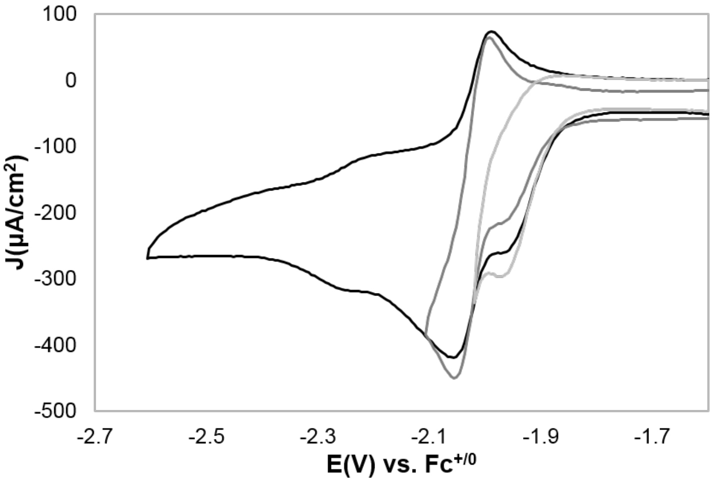

Figure S16: First (light gray), second (gray), and third (black) reduction potentials of **1**. Conditions: 1 mM catalyst in MeCN with 0.1 M $TBAPF_6$. Scan rate: 100 mV/s.

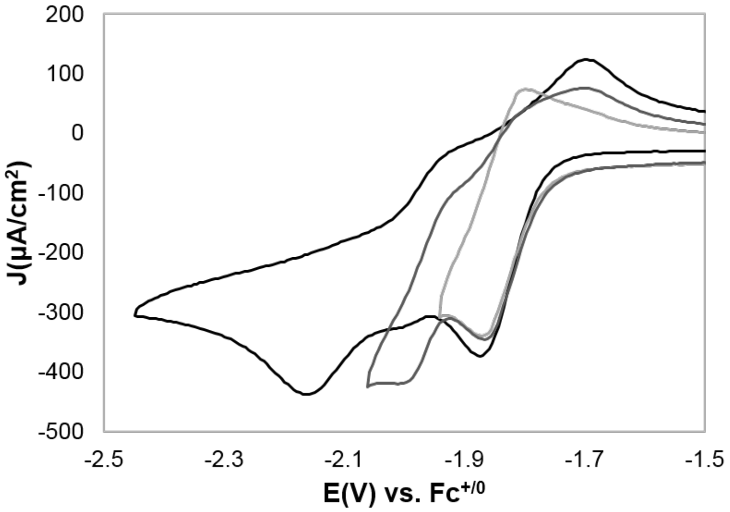

Figure S17: First (light gray), second (dark gray), and third (black) reduction potentials of **2**. Conditions: 1 mM catalyst in MeCN with 0.1 M $TBAPF_6$. Scan rate: 100 mV/s.

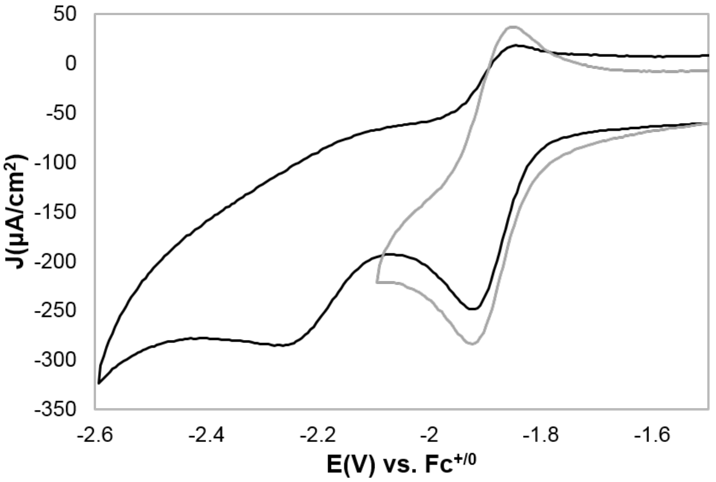

Figure S18: First (gray) and second (black) reduction potentials of **3**. Conditions: 1 mM catalyst in MeCN with 0.1 M $TBAPF_6$. Scan rate: 100 mV/s.

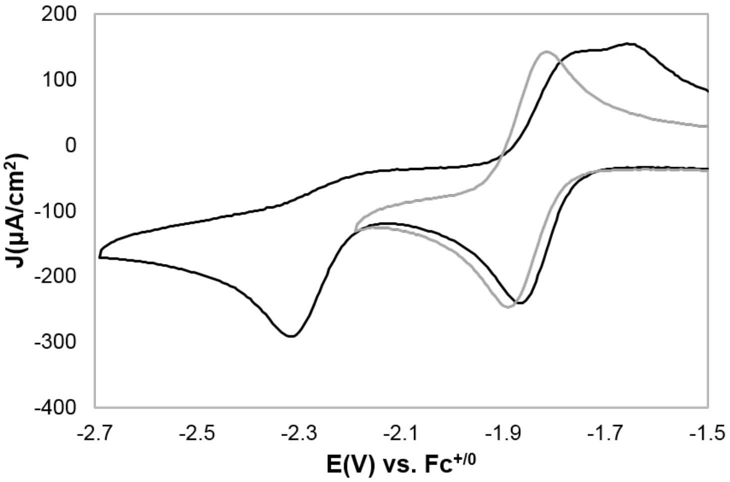

Figure S19: First (gray) and second (black) reduction potentials of **4**. Conditions: 1 mM catalyst in MeCN with 0.1 M $TBAPF_6$. Scan rate: 100 mV/s.

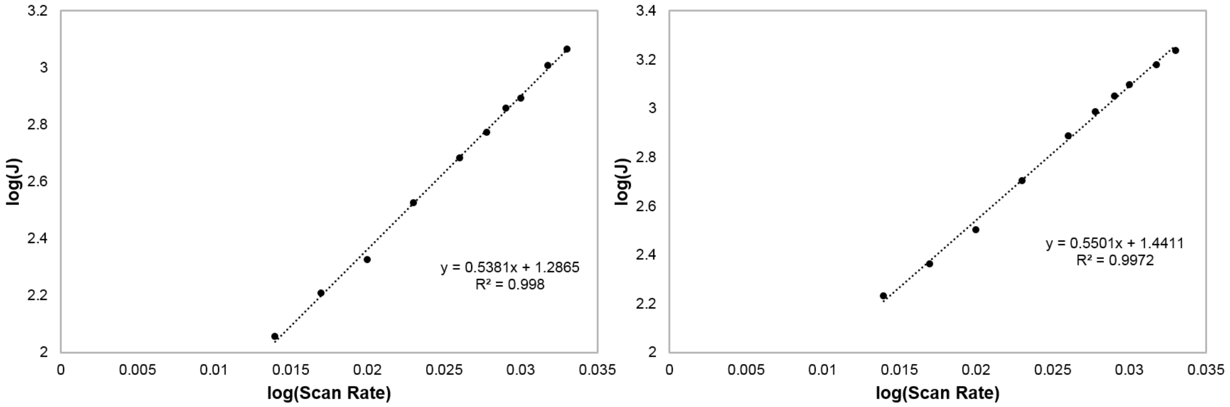

Figure S20: Randles-Sevcik plots for the first (left) and second (right) reductions of **1** at -1.96 and -2.25 V, respectively; the linear correlation and slope of c.a. 0.5 indicates that the species is freely diffusing based on the Randles-Sevcik equation.

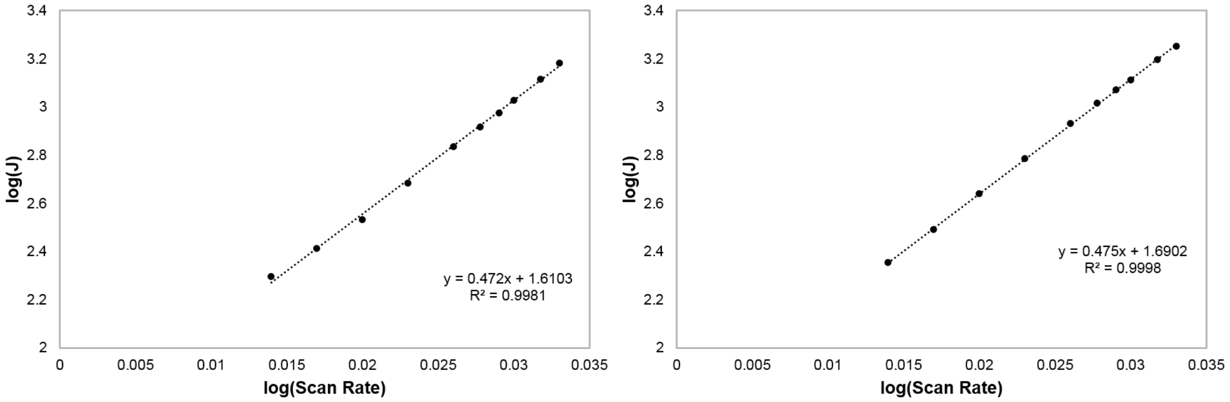

Figure S21: Randles-Sevcik plots for the first (left) and second (right) reductions of **2** at -1.87 and -2.16 V, respectively; the linear correlation indicates that the species is freely diffusing based on the Randles-Sevcik equation.

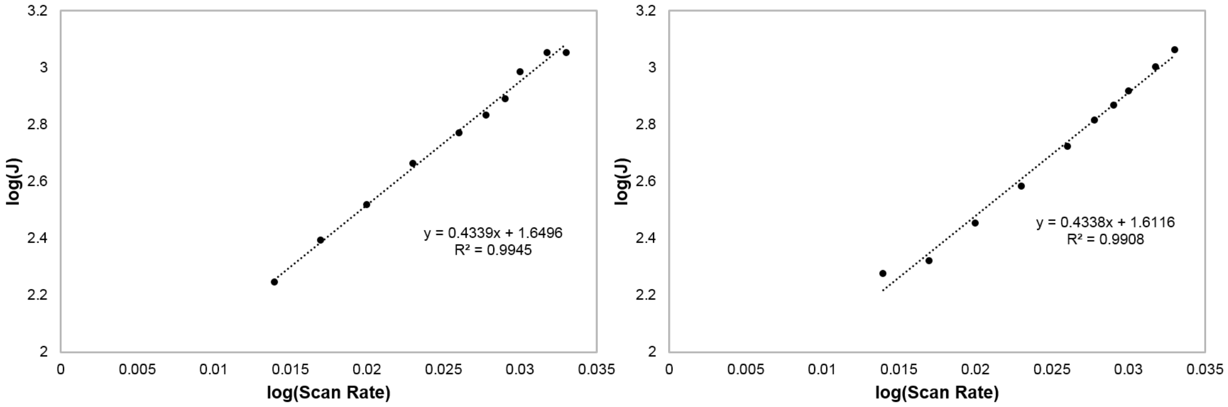

Figure S22: Randles-Sevcik plots versus log(scan rate) for the first (left) and second (right) reductions of **3** at -1.92 and -2.26 V, respectively; the linear correlation indicates that the species is freely diffusing based on the Randles-Sevcik equation.

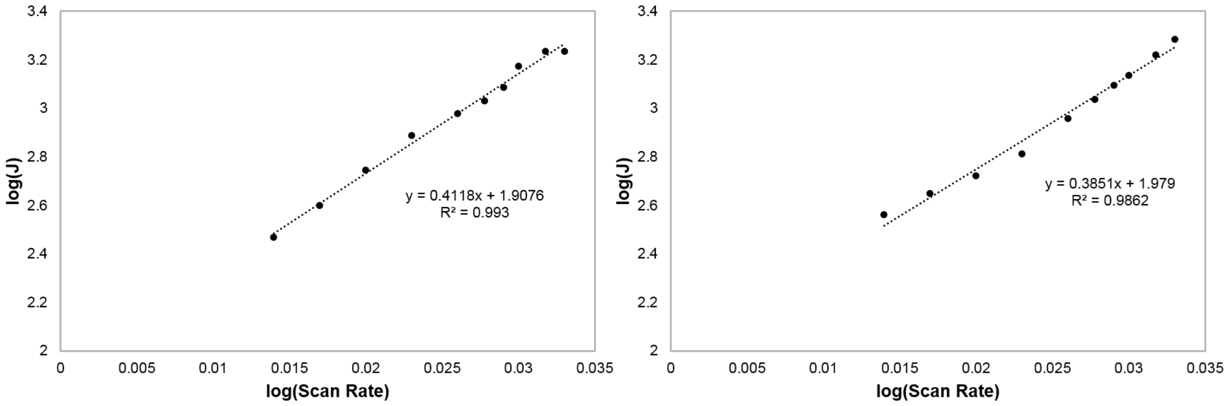

Figure S23: Randles-Sevcik plots versus log(scan rate) for the first (left) and second (right) reductions of **4** at -1.84 and -2.19 V, respectively; the linear correlation indicates that the species is freely diffusing based on the Randles-Sevcik equation.

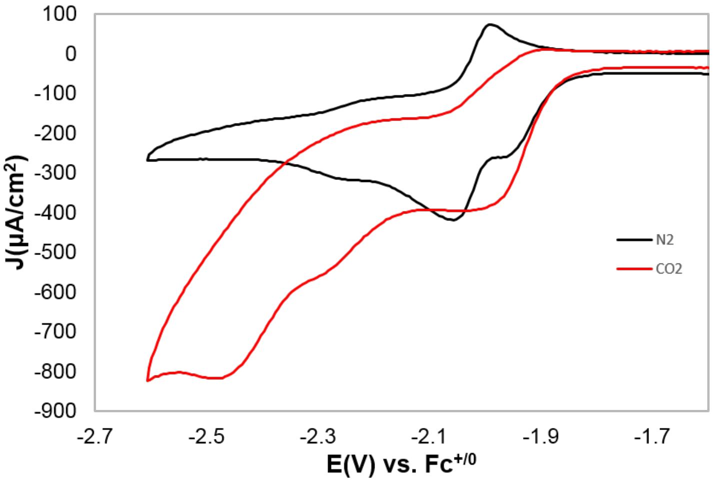

Figure S24: Cyclic voltammogram of **1** under N_2 (black) and CO_2 (red). Conditions: 1 mM catalyst in MeCN with 0.1 M $TBAPF_6$. Scan rate: 100 mV/s.

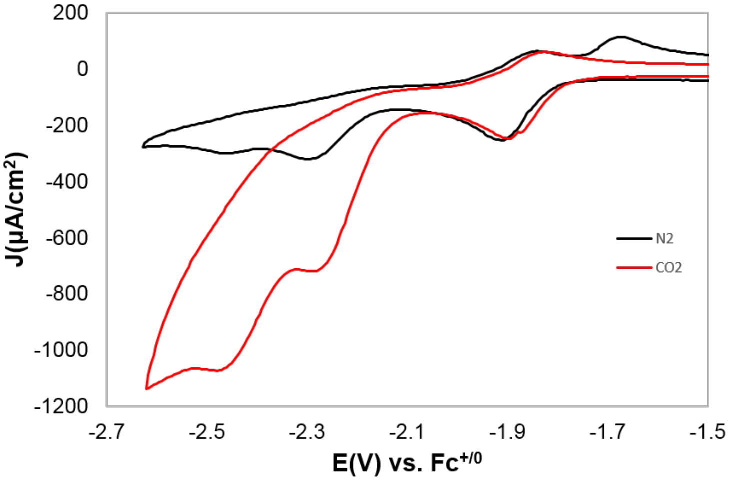

Figure S25: Cyclic voltammogram of **2** under N_2 (black) and CO_2 (red). Conditions: 1 mM catalyst in MeCN with 0.1 M $TBAPF_6$. Scan rate: 100 mV/s.

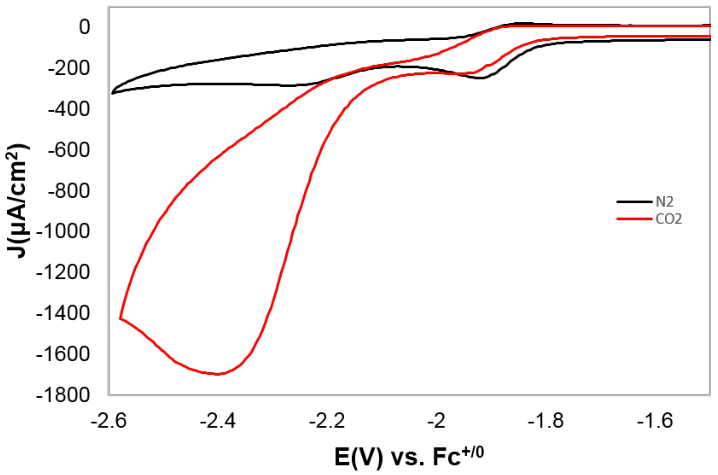

Figure S26: Cyclic voltammogram of **3** under N_2 (black) and CO_2 (red). Conditions: 1 mM catalyst in MeCN with 0.1 M $TBAPF_6$. Scan rate: 100 mV/s.

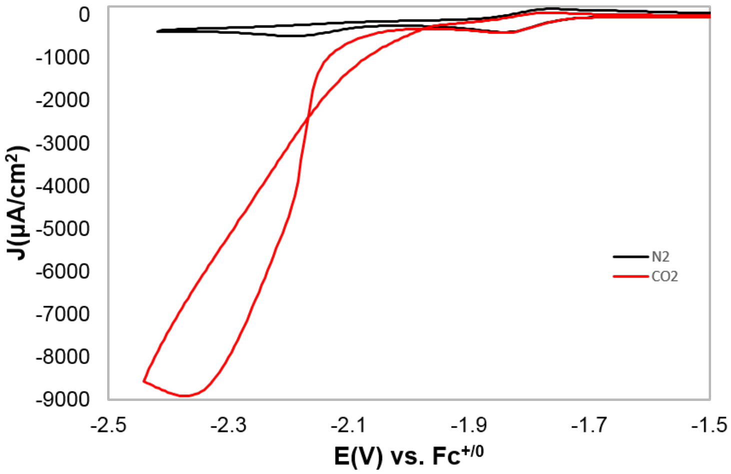

Figure S27: Cyclic voltammogram of **4** under N_2 (black) and CO_2 (red). Conditions: 1 mM catalyst in MeCN with 0.1 M $TBAPF_6$. Scan rate: 100 mV/s.

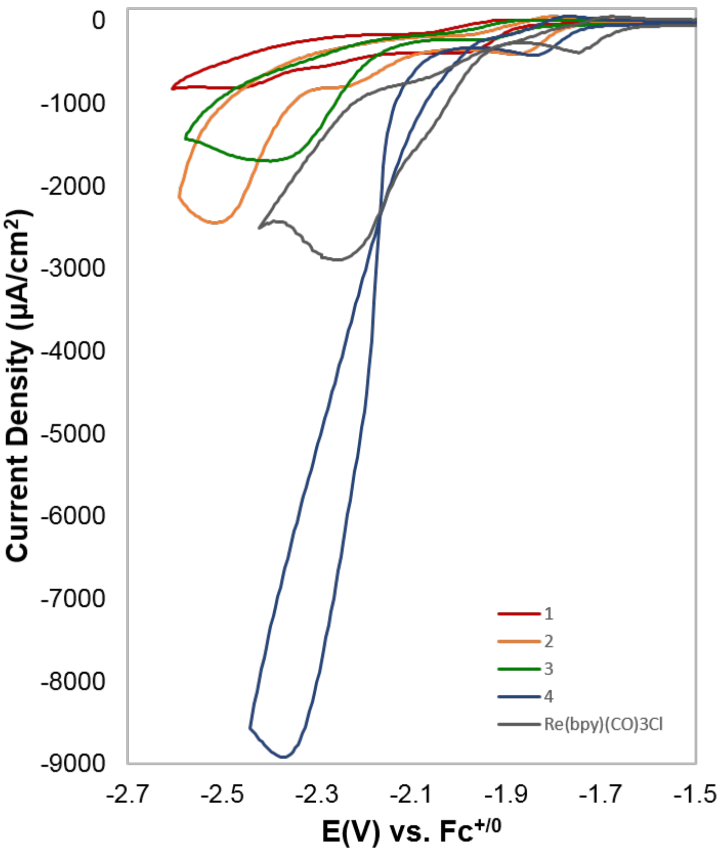

Figure S28: Cyclic voltammograms of **1** (red), **2** (orange), **3** (green), **4** (blue), and Re(bpy)$(CO)_3Cl$ complex (gray) under catalytic conditions (CO_2 atmosphere, 1 mM catalyst in MeCN with 0.1 M $TBAPF_6$). Scan rate: 100 mV/s.

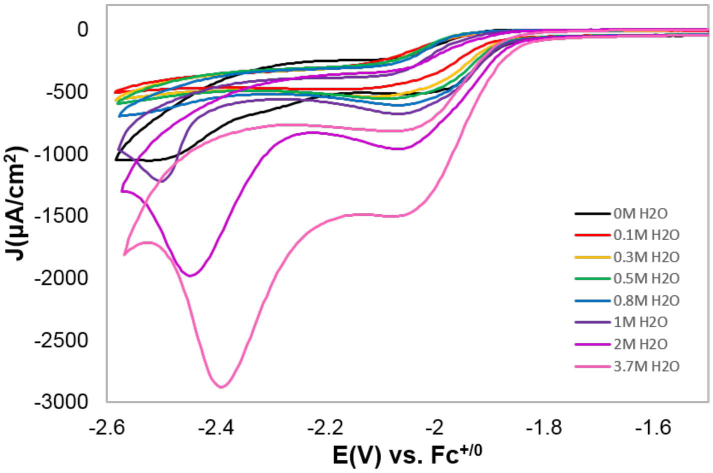

Figure S29: Cyclic voltammograms of **1** under CO_2 with increasing concentrations of H_2O. Conditions: 1 mM catalyst in MeCN with 0.1 M $TBAPF_6$. Scan rate: 100 mV/s.

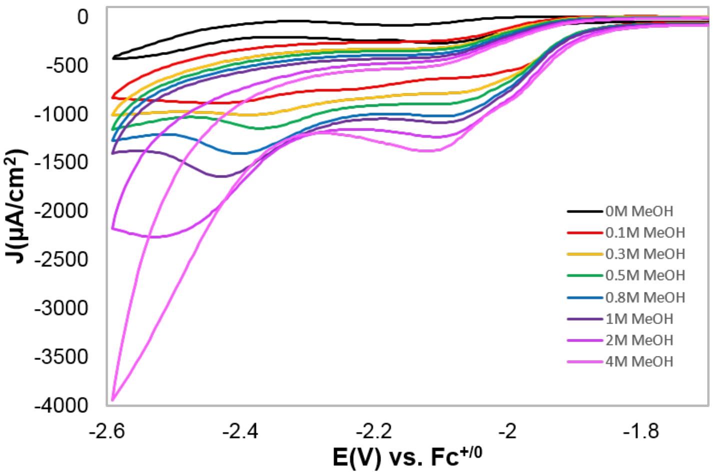

Figure S30: Cyclic voltammograms of **1** under CO_2 with increasing concentrations of MeOH. Conditions: 1 mM catalyst in MeCN with 0.1 M $TBAPF_6$. Scan rate: 100 mV/s.

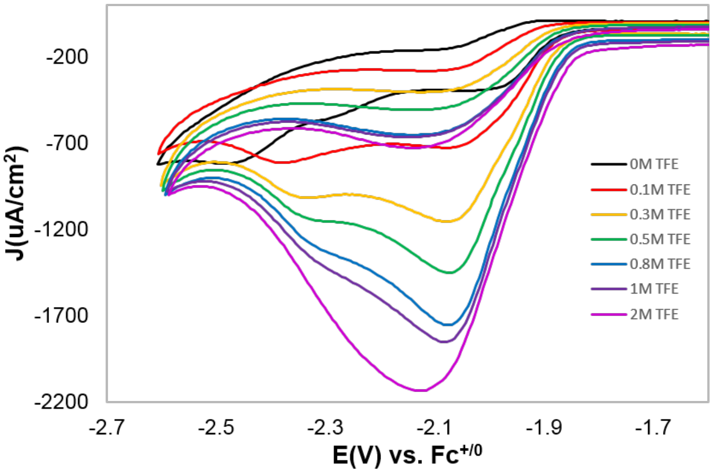

Figure S31: Cyclic voltammograms of **1** under CO_2 with increasing concentrations of TFE. Conditions: 1 mM catalyst in MeCN with 0.1 M $TBAPF_6$. Scan rate: 100 mV/s.

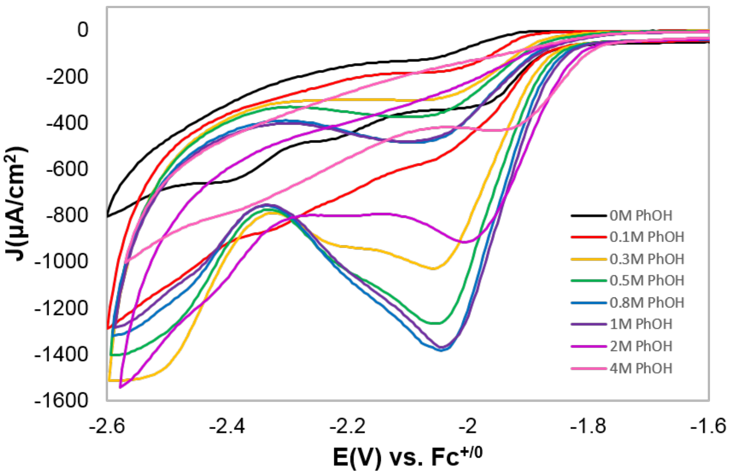

Figure S32: Cyclic voltammograms of **1** under CO_2 with increasing concentrations of PhOH. Conditions: 1 mM catalyst in MeCN with 0.1 M $TBAPF_6$. Scan rate: 100 mV/s.

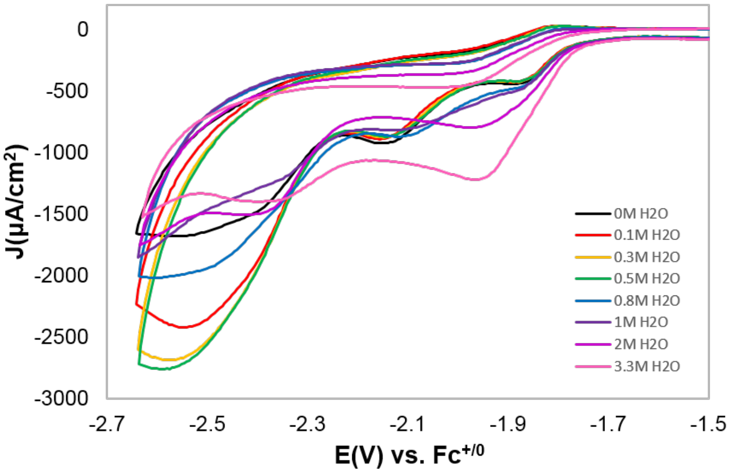

Figure S33: Cyclic voltammograms of **2** under CO_2 with increasing concentrations of H_2O. Conditions: 1 mM catalyst in MeCN with 0.1 M $TBAPF_6$. Scan rate: 100 mV/s.

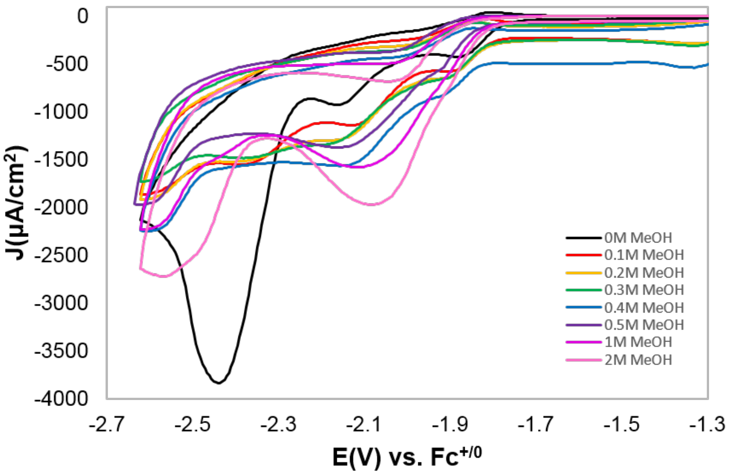

Figure S34: Cyclic voltammograms of **2** under CO_2 with increasing concentrations of MeOH. Conditions: 1 mM catalyst in MeCN with 0.1 M $TBAPF_6$. Scan rate: 100 mV/s.

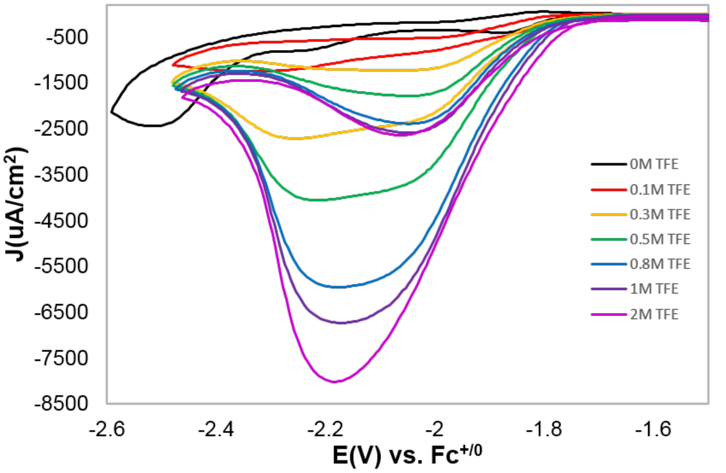

Figure S35: Cyclic voltammograms of **2** under CO_2 with increasing concentrations of TFE. Conditions: 1 mM catalyst in MeCN with 0.1 M $TBAPF_6$. Scan rate: 100 mV/s.

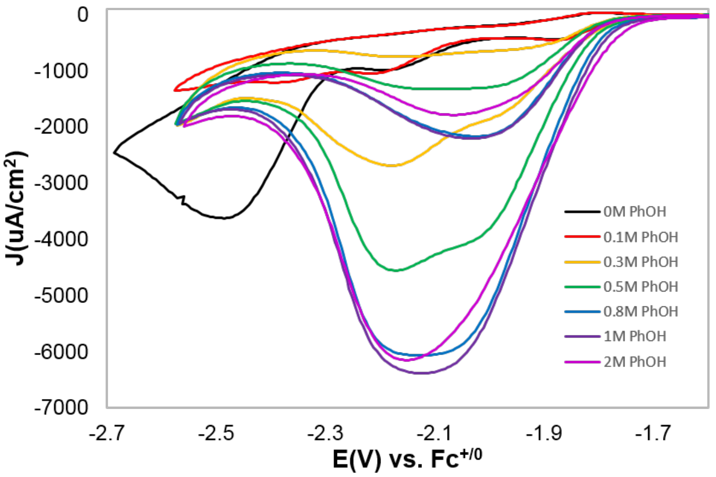

Figure S36: Cyclic voltammograms of **2** under CO_2 with increasing concentrations of PhOH. Conditions: 1 mM catalyst in MeCN with 0.1 M $TBAPF_6$. Scan rate: 100 mV/s.

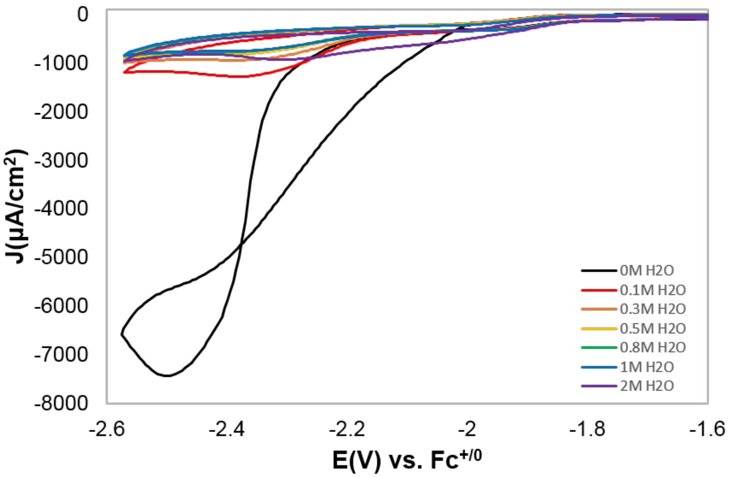

Figure S37: Cyclic voltammograms of **3** under CO_2 with increasing concentrations of H_2O. Conditions: 1 mM catalyst in MeCN with 0.1 M $TBAPF_6$. Scan rate: 100 mV/s.

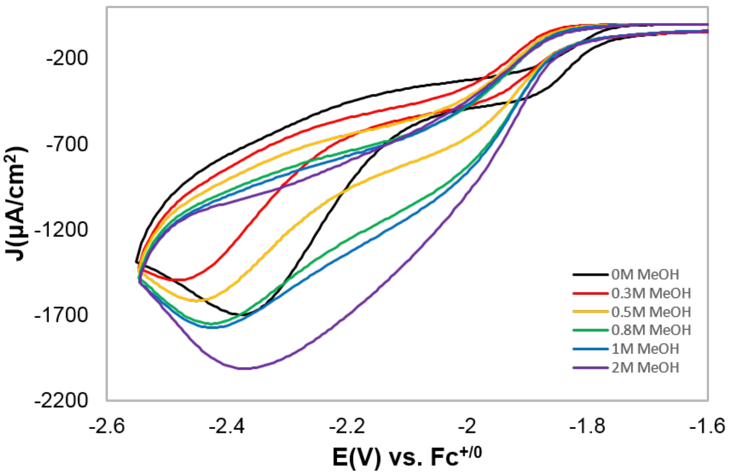

Figure S38: Cyclic voltammograms of **3** under CO_2 with increasing concentrations of MeOH. Conditions: 1 mM catalyst in MeCN with 0.1 M $TBAPF_6$. Scan rate: 100 mV/s.

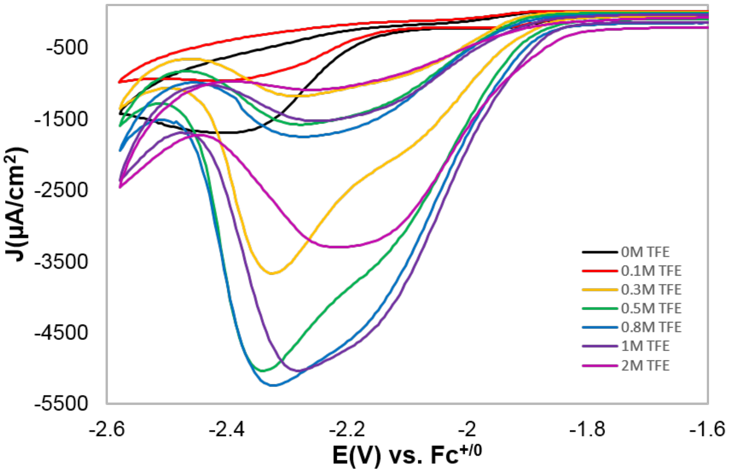

Figure S39: Cyclic voltammograms of **3** under CO_2 with increasing concentrations of TFE. Conditions: 1 mM catalyst in MeCN with 0.1 M $TBAPF_6$. Scan rate: 100 mV/s.

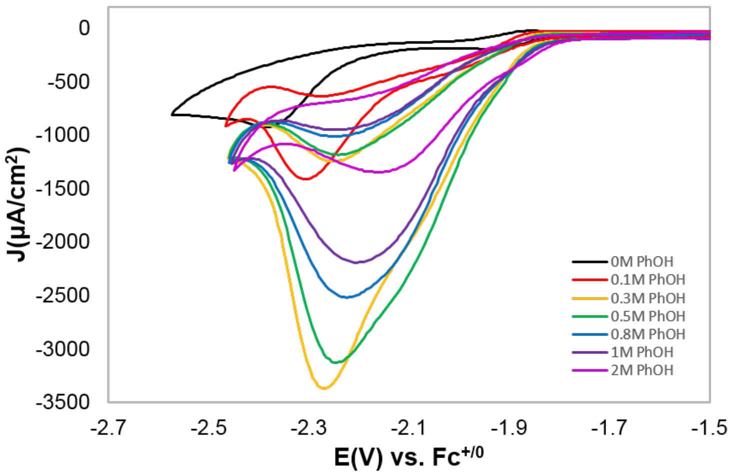

Figure S40: Cyclic voltammograms of **3** under CO_2 with increasing concentrations of PhOH. Conditions: 1 mM catalyst in MeCN with 0.1 M $TBAPF_6$. Scan rate: 100 mV/s.

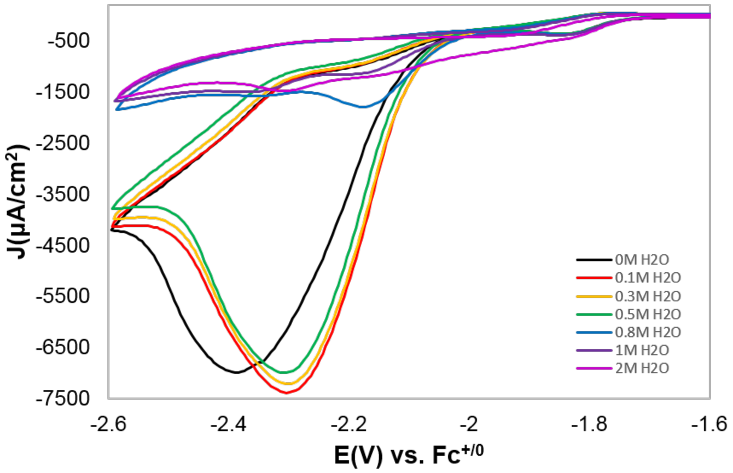

Figure S41: Cyclic voltammograms of **4** under CO_2 with increasing concentrations of H_2O. Conditions: 1 mM catalyst in MeCN with 0.1 M $TBAPF_6$. Scan rate: 100 mV/s.

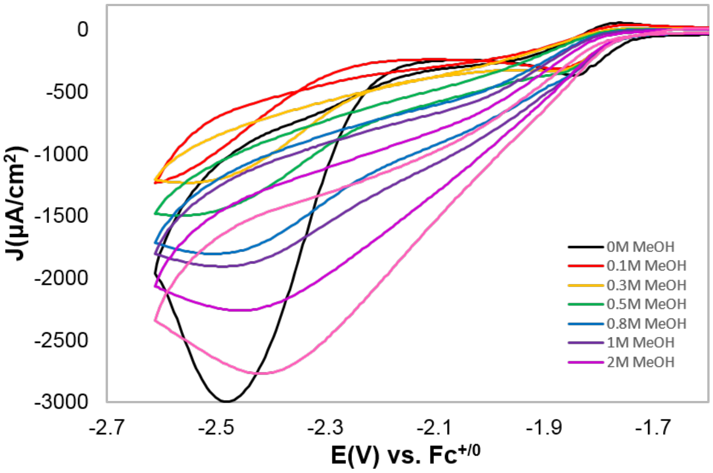

Figure S42: Cyclic voltammograms of **4** under CO_2 with increasing concentrations of MeOH. Conditions: 1 mM catalyst in MeCN with 0.1 M $TBAPF_6$. Scan rate: 100 mV/s.

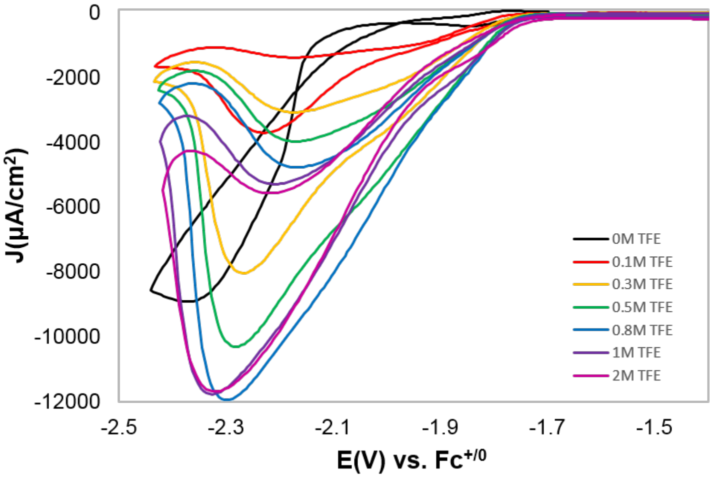

Figure S43: Cyclic voltammograms of **4** under CO_2 with increasing concentrations of TFE. Conditions: 1 mM catalyst in MeCN with 0.1 M $TBAPF_6$. Scan rate: 100 mV/s.

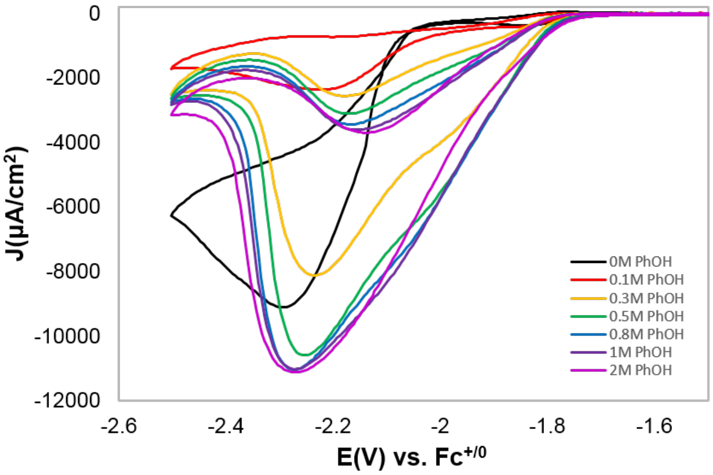

Figure S44: Cyclic voltammograms of **4** under CO_2 with increasing concentrations of PhOH. Conditions: 1 mM catalyst in MeCN with 0.1 M $TBAPF_6$. Scan rate: 100 mV/s.

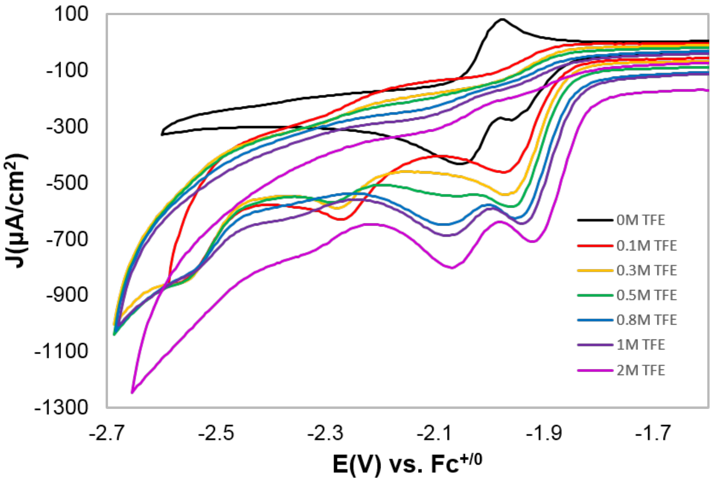

Figure S45: Cyclic voltammograms of **1** under N_2 with increasing amounts of TFE. Conditions: 1 mM catalyst in MeCN with 0.1 M $TBAPF_6$. Scan rate: 100 mV/s.

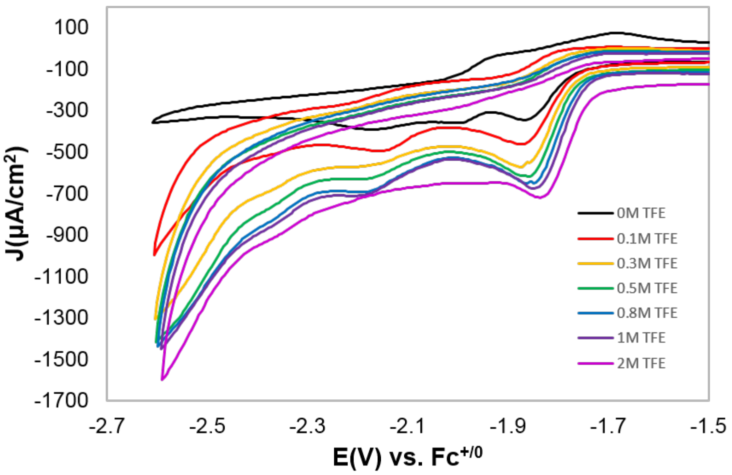

Figure S46: Cyclic voltammograms of **2** under N_2 with increasing amounts of TFE. Conditions: 1 mM catalyst in MeCN with 0.1 M $TBAPF_6$. Scan rate: 100 mV/s.

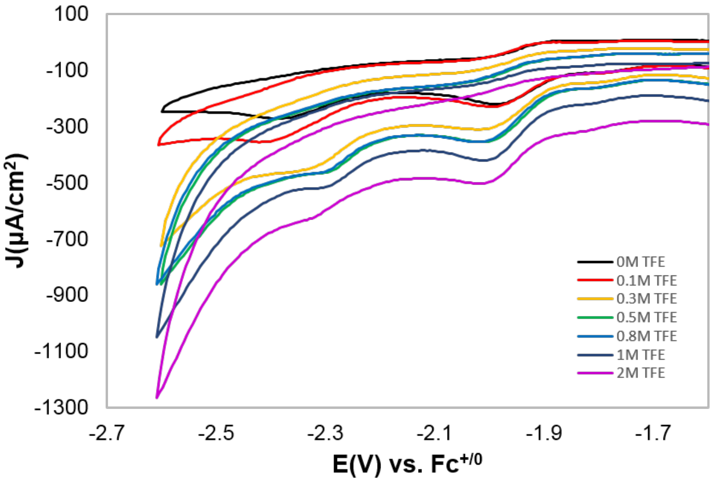

Figure S47: Cyclic voltammograms of **3** under N_2 with increasing amounts of TFE. Conditions: 1 mM catalyst in MeCN with 0.1 M $TBAPF_6$. Scan rate: 100 mV/s.

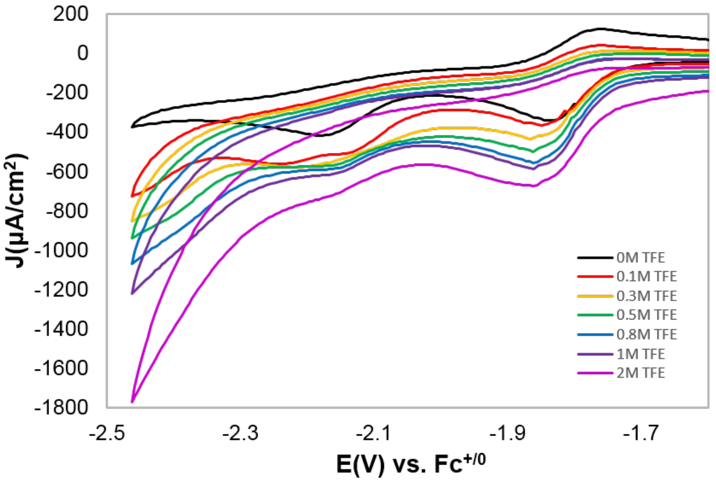

Figure S48: Cyclic voltammograms of **4** under N_2 with increasing amounts of TFE. Conditions: 1 mM catalyst in MeCN with 0.1 M $TBAPF_6$. Scan rate: 100 mV/s.

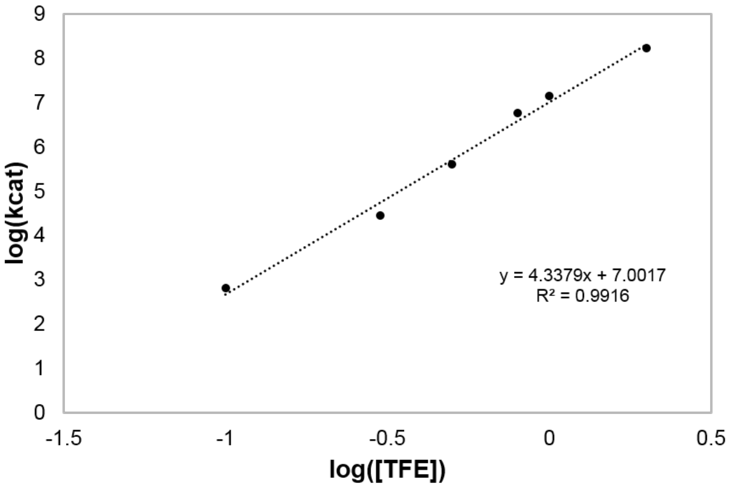

Figure S49: log(k_{cat}) versus log([TFE]) for **1**, showing a linear dependence of rate on acid concentration.

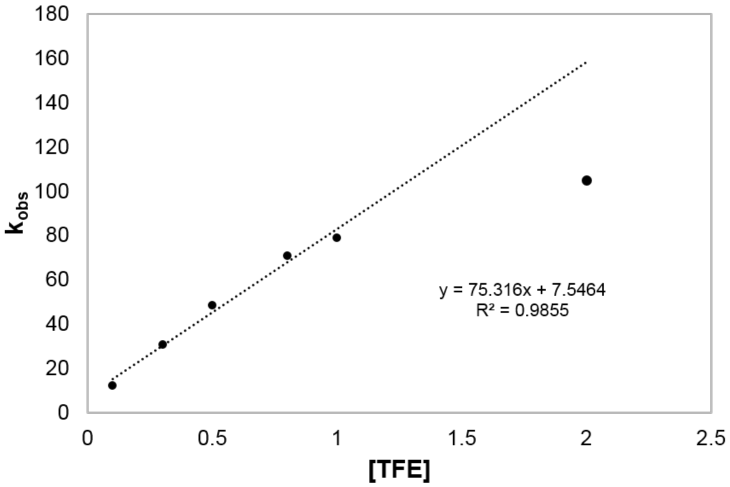

Figure S50: k_{cat} versus acid concentration for **1**; the slope gives a rate of 75 $M^{-1}s^{-1}$.

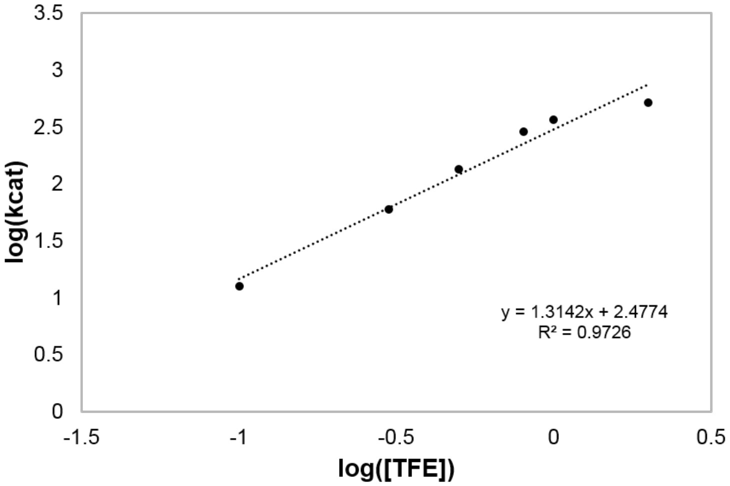

Figure S51: log(k_{cat}) versus log([TFE]) for **2**, showing a linear dependence of rate on acid concentration.

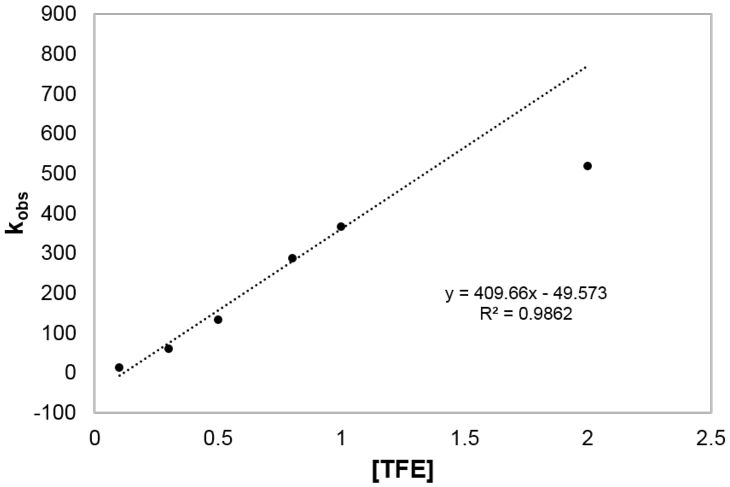

Figure S52: k_{cat} versus acid concentration for **2**; the slope gives a rate of 410 $M^{-1}s^{-1}$.

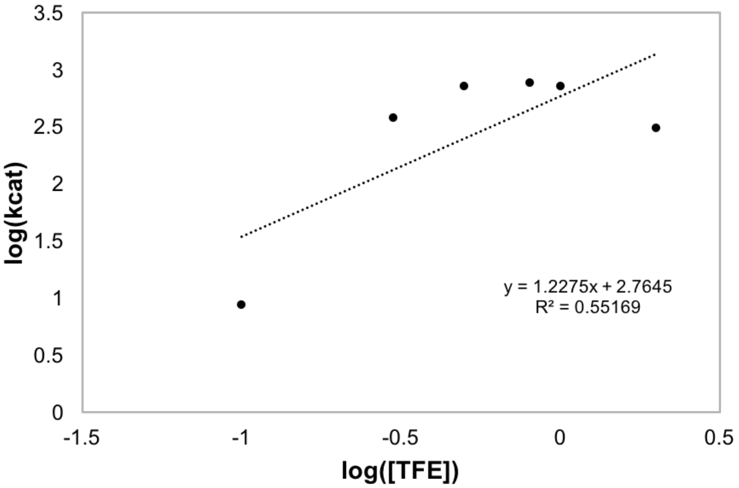

Figure S53: log(k_{cat}) versus log([TFE]) for **3**, showing a non-linear dependence of rate on acid concentration.

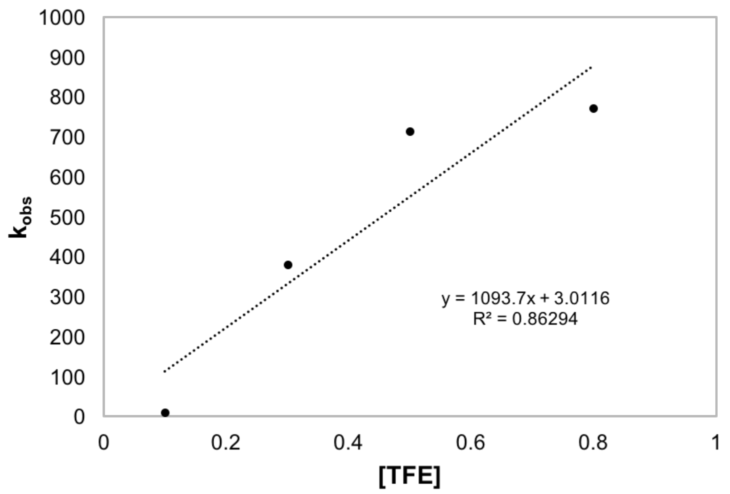

Figure S54: k_{cat} versus acid concentration for **3**, only including concentrations for which the current is increasing; the slope gives a rate of 1094 $M^{-1}s^{-1}$.

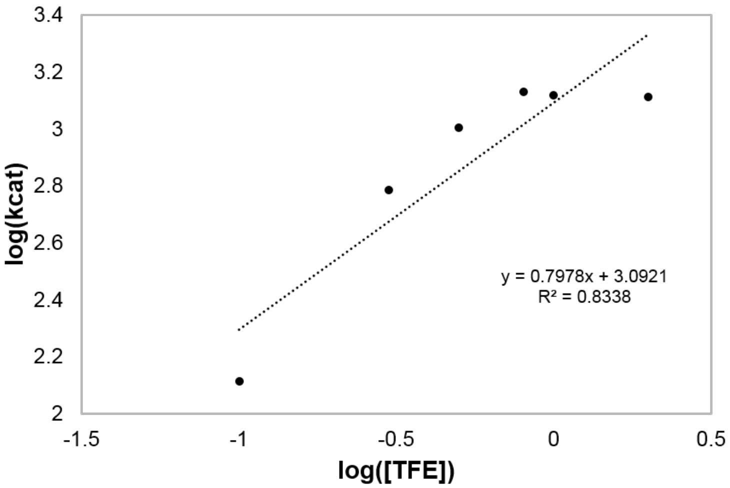

Figure S55: log(k_{cat}) versus log([TFE]) for **4**, showing a linear dependence of rate on acid concentration at lower acid concentrations.

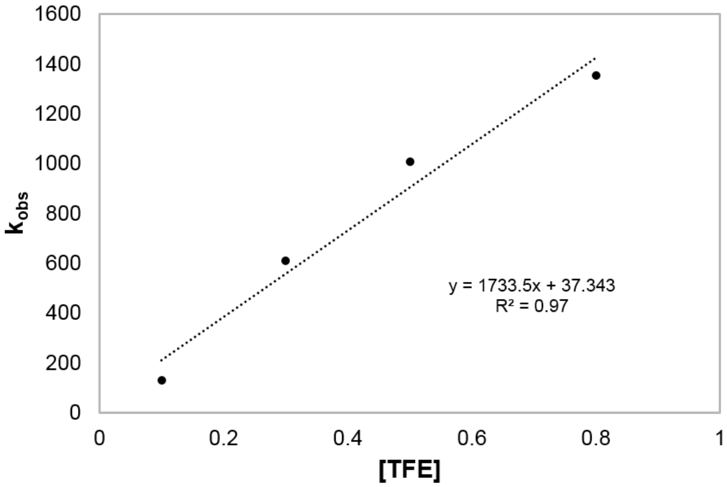

Figure S56: k_{cat} versus acid concentration for **4**; the slope gives a rate of 1734 $M^{-1}s^{-1}$.

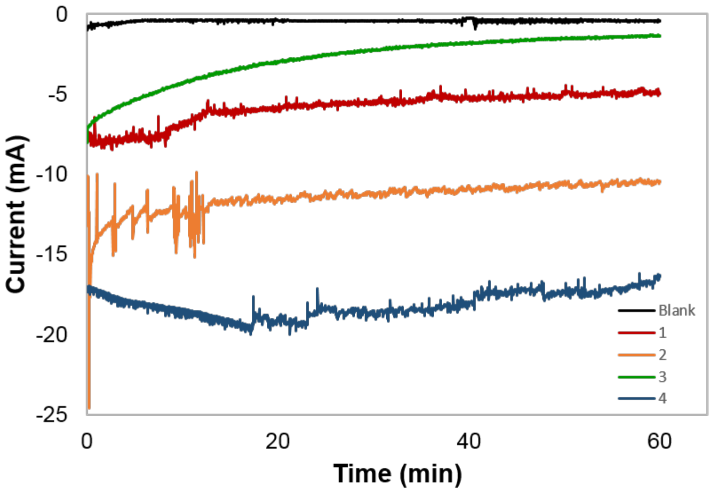

Figure S57: Current versus time over one hour of controlled potential electrolysis for complexes **1** (red)**, 2** (orange), **3** (green), and **4** (blue). BE studies were performed using 1 mM catalyst in MeCN with 0.1 M $TBAPF_6$.

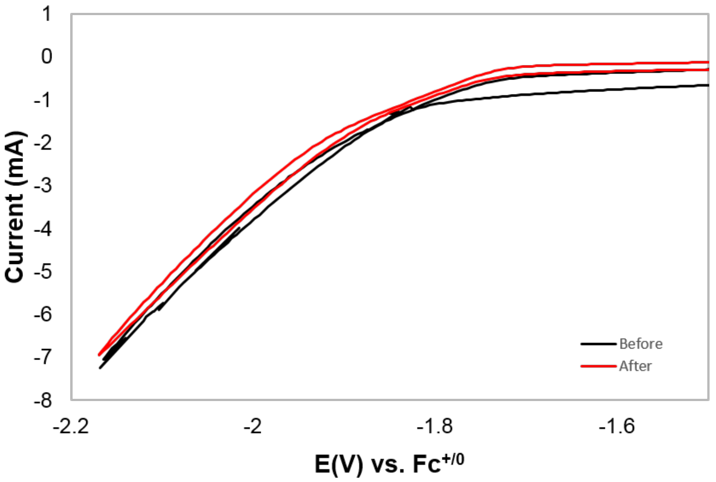

Figure S58: Cyclic voltammograms of **1** before and after controlled potential electrolysis with 2 M TFE, showing a very minimal decrease in current after one hour of electrolysis.

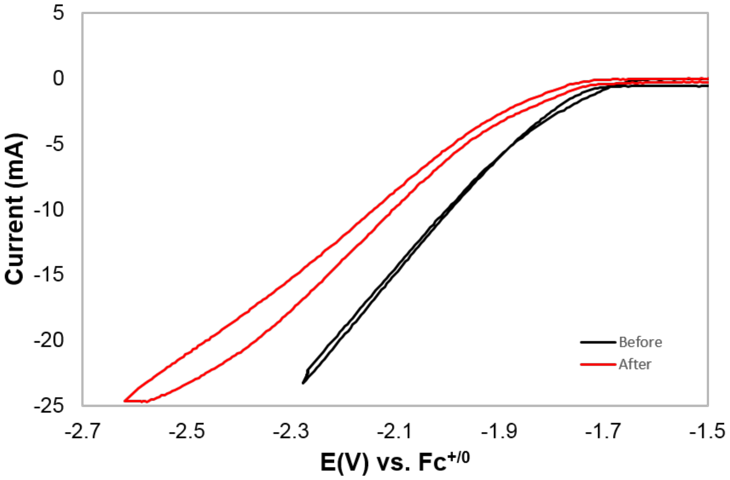

Figure S59: Cyclic voltammograms of **2** before and after controlled potential electrolysis with 2 M TFE, showing a slight decrease in current after one hour of electrolysis.

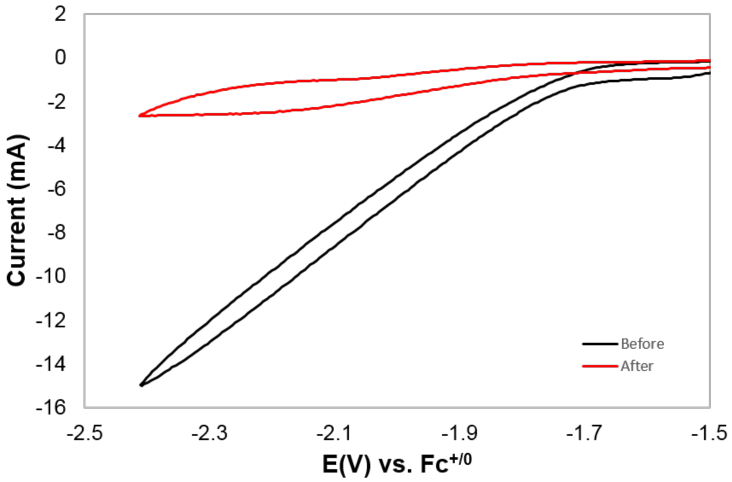

Figure S60: Cyclic voltammograms of **2** before and after controlled potential electrolysis under CO_2 with 2 M PhOH, showing a significant decrease in current after one hour of electrolysis.

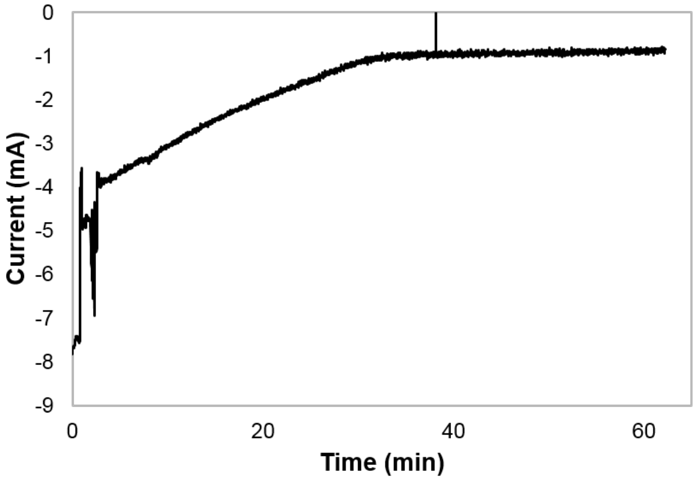

Figure S61: Current versus time of **2** during one hour of controlled potential electrolysis under CO_2 with 2 M PhOH, showing a significant decrease in current over the first 30 minutes.

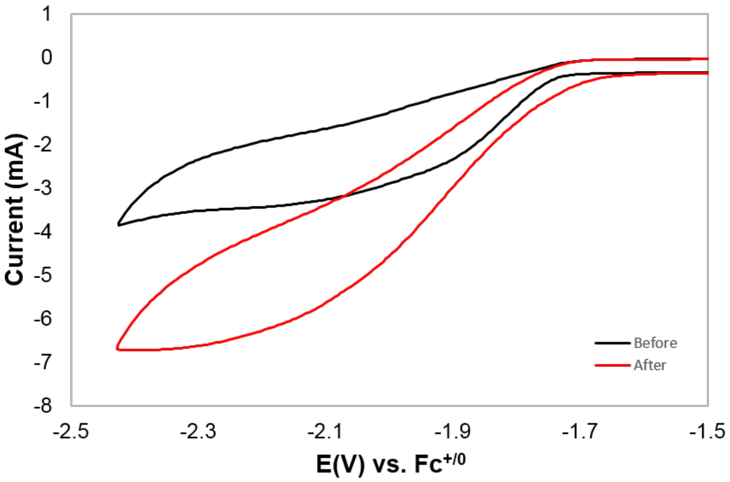

Figure S62: Cyclic voltammograms of **2** before and after controlled potential electrolysis under N_2 with 2 M TFE, showing a slight increase in current after one hour of electrolysis; this current is significantly lower than the current response observed for **2** under CO_2.

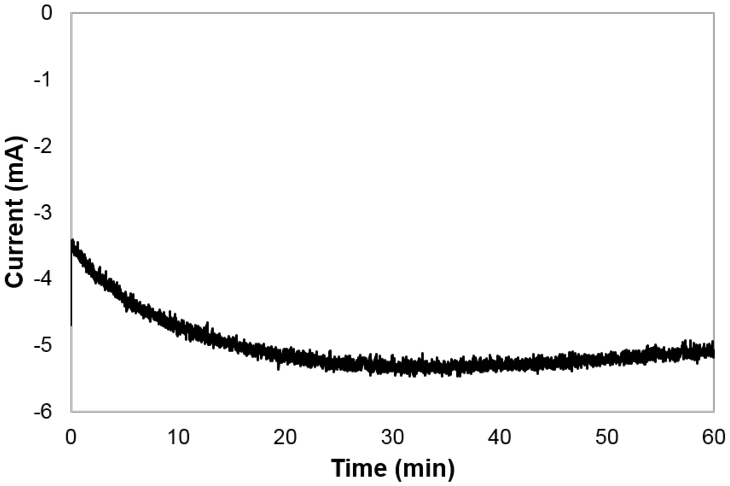

Figure S63: Current versus time of **2** during one hour of controlled potential electrolysis under N_2 with 2 M TFE, showing a lower current response than is observed for the same conditions under CO_2.

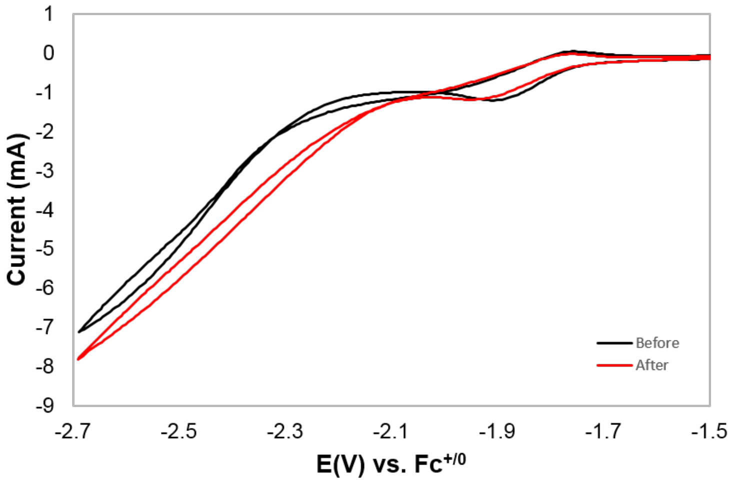

Figure S64: Cyclic voltammograms of **3** before and after controlled potential electrolysis under CO_2 with 2 M TFE, showing a slight increase in current after one hour of electrolysis.

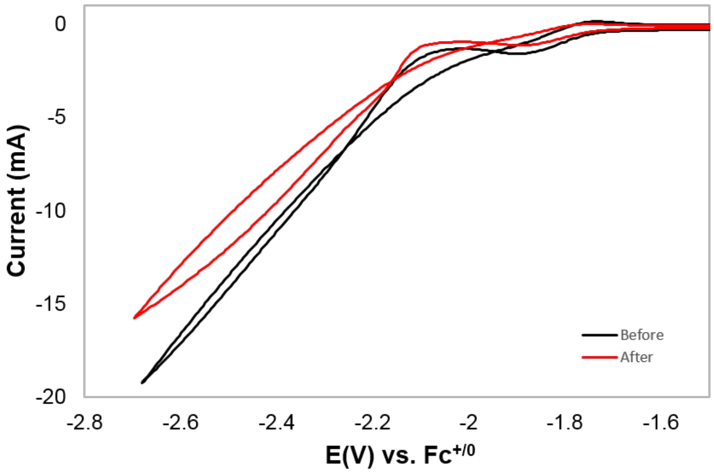

Figure S65: Cyclic voltammograms of **4** before and after controlled potential electrolysis with 2 M TFE, showing a minimal decrease in current after one hour of electrolysis.

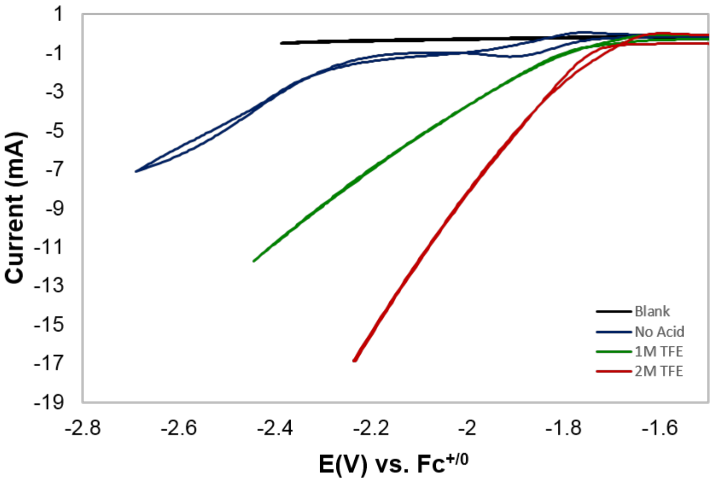

Figure S66: Cyclic voltammograms of a blank cell and **4** before controlled potential electrolysis with no added TFE, 1 M TFE, and 2 M TFE, showing a dependence of catalytic onset and current response on acid concentration.

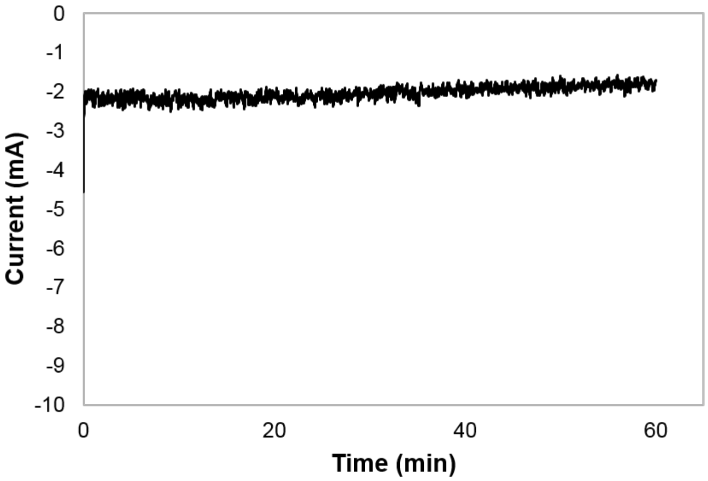

Figure S67: Current versus time of **4** during one hour of controlled potential electrolysis with 2 M TFE under an N_2 atmosphere, showing a significantly lower current response than that observed under CO_2.

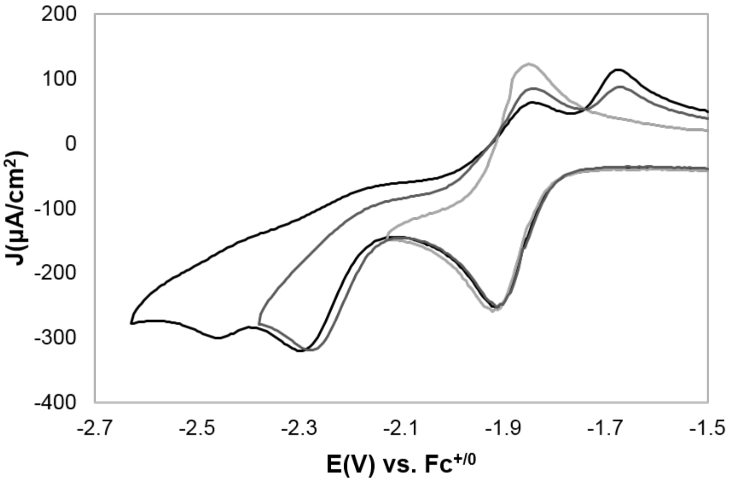

Figure S68: First and second reduction potentials of **2** in DMF. 1 mM catalyst in DMF with 0.1 M $TBAPF_6$, scan rate: 100 mV/s.

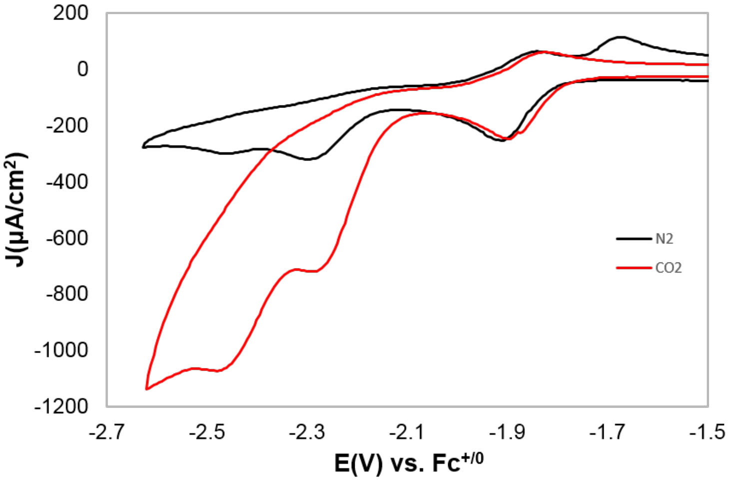

Figure S69: Cyclic voltammogram of **2** in DMF under N_2 compared with that under CO_2. 1 mM catalyst in DMF with 0.1 M $TBAPF_6$, scan rate: 100 mV/s.

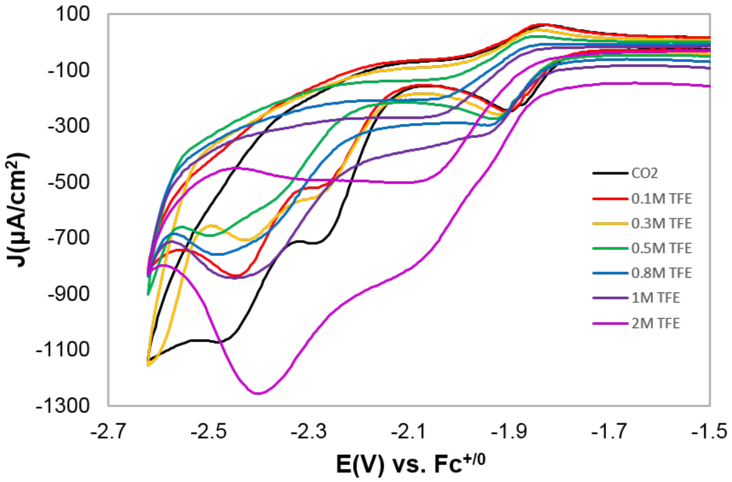

Figure S70: Cyclic voltammograms of **2** under CO_2 with increasing concentrations of TFE. 1 mM catalyst in DMF with 0.1 M $TBAPF_6$, scan rate: 100 mV/s.

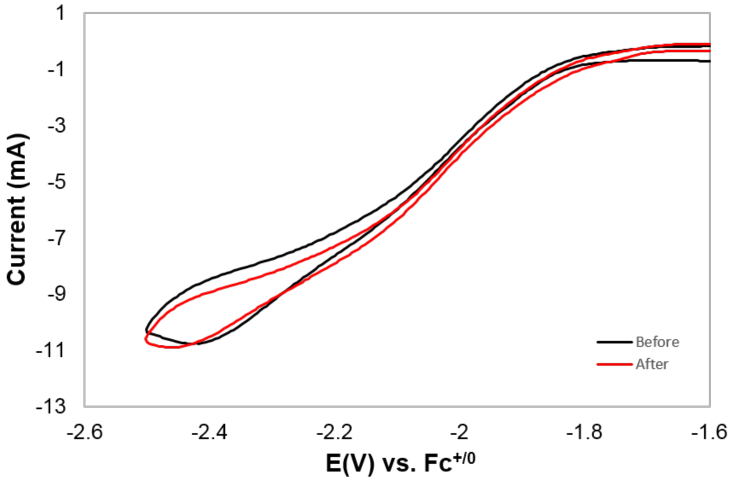

Figure S71: Cyclic voltammograms of **2** before and after controlled potential electrolysis in DMF with 2 M TFE.

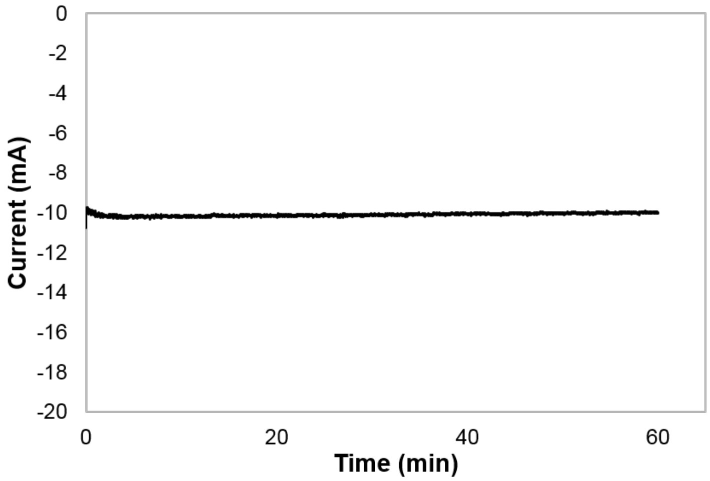

Figure S72: Current versus time of **2** during one hour of controlled potential electrolysis in DMF with 2 M TFE.

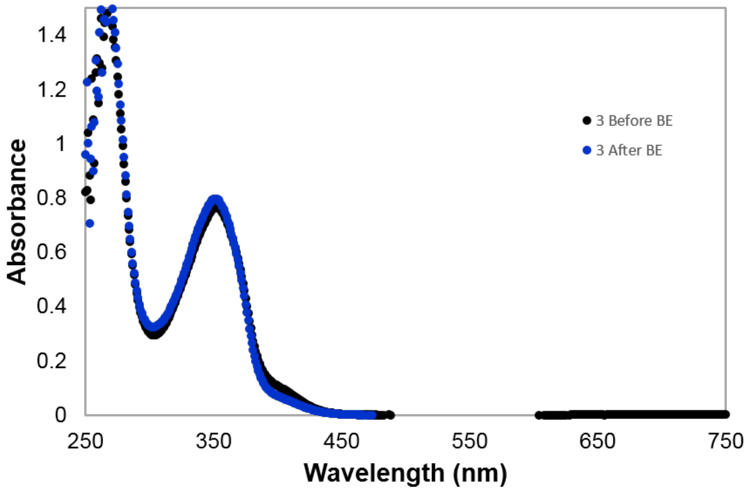

Figure S73: UV-vis before and after CPE of the working solution of the electrolysis cell for complex **3**.

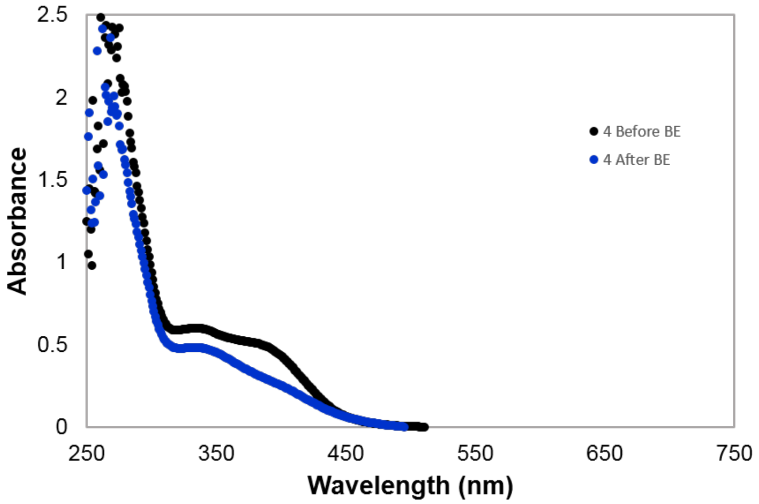

Figure S74: UV-vis before and after CPE of the working solution of the electrolysis cell for complex **4**.

Equation S1. Calculations of total turnover numbers (TON) from CPE studies were performed by using the following equation:

$$\frac{mol\ CO\ produced}{mol\ catalyst\ in\ solution}$$

where mol catalyst in solution is 1 mM = 0.00004 mol in 40 mL solution.

Table S3. Crystal data and structure refinement for **1**.

Chemical formula	$C_{18}H_{21}ClN_5O_4Re$	
Formula weight	593.05 g/mol	
Temperature	100(2) K	
Wavelength	0.71073 Å	
Crystal size	0.085 × 0.163 × 0.168 mm	
Crystal habit	clear light yellow prism	
Crystal system	triclinic	
Space group	$P\bar{1}$	
Unit cell dimensions	a = 8.953(3) Å	α = 80.373(4)°
	b = 9.085(3) Å	β = 76.566(4)°
	c = 13.399(4) Å	γ = 78.668(4)°
Volume	1030.9(5) $Å^3$	
Z	2	
Density (calculated)	1.911 g/cm^3	
Absorption coefficient	6.058 mm^{-1}	
F(000)	576	
Diffractometer	Bruker APEX DUO	
Radiation source	fine-focus tube, MoKα	
Theta range for data collection	1.58 to 30.59°	
Index ranges	$-12 \le h \le 12$, $-12 \le k \le 12$, $-19 \le l \le 19$	
Reflections collected	25548	
Independent reflections	6210 [R(int) = 0.0470]	
Coverage of independent reflections	98.0%	
Absorption correction	multi-scan	
Max. and min. transmission	0.6270 and 0.4290	
Structure solution technique	direct methods	
Structure solution program	SHELXTL XT 2014/4 (Bruker AXS, 2014)	
Refinement method	Full-matrix least-squares on F^2	
Refinement program	SHELXL-2014/6 (Sheldrick, 2014)	
Function minimized	$\Sigma w(F_o^2 - F_c^2)^2$	
Data / restraints / parameters	6210 / 2 / 272	
Goodness-of-fit on F^2	1.068	
Δ/σmax	0.002	
Final R indices	5716 data; $I > 2\sigma(I)$	R_1 = 0.0219, wR_2 = 0.0488
	All data	R_1 = 0.0259, wR_2 = 0.0501
Weighting scheme	$w=1/[\sigma^2(F_o^2)+(0.0147P)^2+0.5921P]$ where $P = (F_o^2+2F_c^2)/3$	
Largest diff. peak and hole	0.972 and -1.081 $eÅ^{-3}$	
R.M.S. deviation from mean	0.130 $eÅ^{-3}$	

Table S4. Crystal data and structure refinement for **2**.

Identification code	Ashley012918	
Chemical formula	$C_{17}H_{18}ClN_4O_4Re$	
Formula weight	564.00 g/mol	
Temperature	103(2) K	
Wavelength	0.71073 Å	
Crystal size	0.089 × 0.258 × 0.322 mm	
Crystal habit	clear light yellow prism	
Crystal system	triclinic	
Space group	$P\overline{1}$	
Unit cell dimensions	a = 8.912(3) Å	α = 84.241(5)°
	b = 8.957(3) Å	β = 87.294(5)°
	c = 12.030(4) Å	γ = 79.875(5)°
Volume	940.1(5) $Å^3$	
Z	2	
Density (calculated)	1.992 g/cm^3	
Absorption coefficient	6.636 mm^{-1}	
F(000)	544	
Diffractometer	Bruker APEX DUO	
Radiation source	fine-focus tube, MoKα	
Theta range for data collection	1.70 to 30.60°	
Index ranges	$-12 \le h \le 12$, $-12 \le k \le 12$, $-16 \le l \le 17$	
Reflections collected	23077	
Independent reflections	5677 [R(int) = 0.0488]	
Coverage of independent reflections	97.9%	
Absorption correction	multi-scan	
Structure solution technique	direct methods	
Structure solution program	SHELXTL XT 2014/5 (Bruker AXS, 2014)	
Refinement method	Full-matrix least-squares on F^2	
Refinement program	SHELXTL XL 2016/6 (Bruker AXS, 2016)	
Function minimized	$\Sigma\, w(F_o^2 - F_c^2)^2$	
Data / restraints / parameters	5677 / 0 / 250	
Goodness-of-fit on F^2	1.072	
Δ/σ_{max}	0.003	
Final R indices	5501 data; $I > 2\sigma(I)$	R_1 = 0.0198, wR_2 = 0.0495
	all data	R_1 = 0.0206, wR_2 = 0.0499
Weighting scheme	$w=1/[\sigma^2(F_o^2)+(0.0150P)^2+0.7497P]$ where $P=(F_o^2+2F_c^2)/3$	
Largest diff. peak and hole	0.903 and -1.492 $eÅ^{-3}$	
R.M.S. deviation from mean	0.135 $eÅ^{-3}$	

Table S5. Crystal data and structure refinement for **3**.

Identification code	Ashley_bisNMe2	
Chemical formula	$C_{18}H_{19}Cl_4N_4O_3Re$	
Formula weight	667.37 g/mol	
Temperature	100(2) K	
Wavelength	0.71073 Å	
Crystal size	0.020 × 0.100 × 0.130 mm	
Crystal system	triclinic	
Space group	$P\overline{1}$	
Unit cell dimensions	a = 9.368(5) Å	α = 75.978(9)°
	b = 11.275(6) Å	β = 76.488(8)°
	c = 11.587(6) Å	γ = 81.595(8)°
Volume	1149.3(11) $Å^3$	
Z	2	
Density (calculated)	1.928 g/cm^3	
Absorption coefficient	5.778 mm^{-1}	
F(000)	644	
Diffractometer	Bruker APEX DUO	
Radiation source	fine-focus tube (MoKα , λ = 0.71073 Å)	
Theta range for data collection	1.85 to 28.07°	
Reflections collected	7978	
Coverage of independent reflections	94.9%	
Absorption correction	multi-scan	
Max. and min. transmission	0.8890 and 0.5090	
Structure solution technique	direct methods	
Structure solution program	SHELXTL XT 2014/5 (Bruker AXS, 2014)	
Refinement method	Full-matrix least-squares on F^2	
Refinement program	SHELXTL XL 2018/3 (Bruker AXS, 2018)	
Function minimized	Σ w(F_o^2 - F_c^2)^2	
Data / restraints / parameters	7978 / 261 / 277	
Goodness-of-fit on F^2	1.028	
Final R indices	5841 data; $I > 2\sigma(I)$	R_1 = 0.1016, wR_2 = 0.2579
	all data	R_1 = 0.1429, wR_2 = 0.2963
Weighting scheme	$w=1/[\sigma^2(F_o^2)+(0.1896P)^2+29.3759P]$ where $P=(F_o^2+2F_c^2)/3$	
Largest diff. peak and hole	11.085 and -6.164 $eÅ^{-3}$	
R.M.S. deviation from mean	0.526 $eÅ^{-3}$	

Table S6. Crystal data and structure refinement for **4**.

Identification code	Ashley082218	
Chemical formula	$C_{15}H_{13}ClN_3O_3Re$	
Formula weight	504.93 g/mol	
Temperature	100(2) K	
Wavelength	0.71073 Å	
Crystal size	0.200 × 0.242 × 0.352 mm	
Crystal habit	clear orange prism	
Crystal system	triclinic	
Space group	$P\overline{1}$	
Unit cell dimensions	a = 7.333(2) Å	α = 91.690(4)°
	b = 8.821(3) Å	β = 99.041(4)°
	c = 13.059(4) Å	γ = 107.903(4)°
Volume	791.1(4) $Å^3$	
Z	2	
Density (calculated)	2.120 g/cm^3	
Absorption coefficient	7.866 mm^{-1}	
F(000)	480	
Diffractometer	Bruker APEX DUO	
Radiation source	fine-focus tube, MoKα	
Theta range for data collection	1.58 to 30.64°	
Index ranges	$-10 \leq h \leq 10$, $-12 \leq k \leq 12$, $-18 \leq l \leq 18$	
Reflections collected	19445	
Independent reflections	4782 [R(int) = 0.0340]	
Coverage of independent reflections	97.8%	
Absorption correction	multi-scan	
Max. and min. transmission	0.3020 and 0.1680	
Structure solution technique	direct methods	
Structure solution program	SHELXTL XT 2014/4 (Bruker AXS, 2014)	
Refinement method	Full-matrix least-squares on F^2	
Refinement program	SHELXTL XL 2014/7 (Bruker AXS, 2014)	
Function minimized	$\Sigma\, w(F_o^2 - F_c^2)^2$	
Data / restraints / parameters	4782 / 0 / 210	
Goodness-of-fit on F^2	1.087	
Δ/σ_{max}	0.003	
Final R indices	4686 data; $I > 2\sigma(I)$	R_1 = 0.0157, wR_2 = 0.0381
	all data	R_1 = 0.0162, wR_2 = 0.0384
Weighting scheme	$w=1/[\sigma^2(F_o^2)+(0.0114P)^2+0.5504P]$ where $P=(F_o^2+2F_c^2)/3$	
Largest diff. peak and hole	0.947 and -1.237 $eÅ^{-3}$	
R.M.S. deviation from mean	0.117 $eÅ^{-3}$	

Table S7. Nitrogen–rhenium bond lengths (in Ångstroms) for complexes **1**, **2**, and **4**.

Complex	**Re—N$_1$(pyridine)**	**Re—N$_2$(pyridine)**
1	2.194(2)	2.202(2)
2	2.175(2)	2.200(2)
4	2.1624(17)	2.2255(17)